

# Thermodynamically Consistent Diffuse Interface Model for Cell Adhesion and Aggregation

Lingyue Shen<sup>a</sup>, Ping Lin<sup>a</sup>, Zhiliang Xu<sup>b</sup>, Shixin Xu<sup>c,\*</sup>

<sup>a</sup>*Department of Mathematics, University of Dundee, Dundee DD1 4HN, Scotland, United Kingdom.*

<sup>b</sup>*Department of Applied and Computational Mathematics and Statistics, University of Notre Dame, 102G Crowley Hall, Notre Dame, IN 46556*

<sup>c</sup>*Duke Kunshan University, 8 Duke Ave, Kunshan, Jiangsu, China.*

---

## Abstract

A thermodynamically consistent phase-field model is introduced for simulating multicellular deformation, aggregation under flow conditions. In particular, a Lennard-Jones type potential is proposed under phase field framework for cell-cell, cell-wall interactions. A second-order accurate in both space and time  $C^0$  finite element method is proposed to solve the model governing equations. Various numerical tests confirm the convergence, energy stability, and nonlinear mechanical properties of cells of the proposed scheme. Vesicles with different adhesion are also used to explain the pathological risk for patient with sickle cell disease.

*Keywords:* Vesicle; Aggregation; Energy stable scheme; Cell-wall interaction.

---

## 1. Introduction

Studying interaction between structures (cell-cell and cell-blood-vessel) is an important subject for understanding hemodynamics, because structural interactions at the cellular level unambiguously appear in a broad spectrum of blood flow related problems ranging from red blood cell (RBC) distribution [1] in blood vessel, the growth of blood clot [2], blood cell aggregation [3], sickle cell disease [4], tumor cell dynamics [5] and diabetes [6].

Under the framework of sharp interface description in which interfaces separating different components of matter are idealized as hypersurfaces with zero thickness, there are a number of studies focusing on modeling cell-cell and cell-blood-vessel interactions under blood flow conditions. Following the seminal work of Peskin [7, 8], the immersed boundary method was used to develop a model for platelet aggregation in [9]. Cell-wall interaction model is introduced in [5] to simulate the adhesion and deformation of tumor cells at the vessel wall. Local and non-local models are described in [10] to investigate the invasion and growth of tumor cells. Cell-cell interaction modeling at the micro-scale is carried out in [11, 12, 13, 14] to study the RBC aggregation problem. Multi-scale models are introduced in [15, 16] in which dissipative particle dynamics (DPD) is used in [15] to establish a blood cell model in blood flow and a stochastic cellular potts model (CPM) is introduced in [16] for studying blood clot growth. In [17, 18, 19], to account for cell-cell or cell-substrate adhesion, a Lennard-Jones type potential is introduced as a one dimensional function of the distance between the points on different cell membranes and substrates. The potential is a combination of a repulsive part and an attractive part which shows repulsion when particles get too close and shows attraction when the distance increase. In [18], this potential in combination with DPD method as mentioned before, is utilized to study cell deformation and doublet suspension.

In this work, we focus on utilizing diffuse interface method, also commonly known as phase-field approach [20] to model cell-cell and cell-blood-vessel interactions under blood flow conditions. The phase-field models

---

\*Corresponding author

*Email address:* shixin.xu@dukekunshan.edu.cn (Shixin Xu)

replace the sharp interface description with a thin transition region in which microscopic mixing of the macroscopically distinct components of matter is permitted. The phase-field approach not only yields systems of governing equations that are better amenable to further analysis, but also handles topological changes of the interface naturally [21, 20, 22, 23]. By treating the cell membrane as a diffuse interface, several phase-field vesicle interaction models have been reported recently. Fusion of cellular aggregates in biofabrication is modelled with a single phase-field function in [24]. Vesicle-substrate adhesion model is established in [25, 26, 27] where two phase-field functions are used to indicate wall and vesicle, respectively. Vesicle-vesicle adhesion model is introduced in [28] in which different phase-field functions are used to represent different vesicles. Further, multiple cell aggregation model and simulations are reported in [29, 30].

Numerically simulating cell models with phase-field method is challenging. finite difference method is used in [31] to study the elastic bending energy of the vesicle. Finite element method is introduced in [32, 26, 33, 29], spectral methods with an adequate number of Fourier modes is used in [28, 34]. However, few works developing energy stable numerical schemes are reported for vesicle or cell models, despite the fact that most phase-field models obey energy dissipation law at the continuous level. It is well-known that preserving a discrete counterpart of the energy dissipation property of the system in numerical solution is crucial for long term stability of numerical computation [35, 36]. In this paper, we also try to develop a numerical scheme retaining discrete energy dissipation law that is consistent with the continuous one.

The purposes of this paper is twofold. The first goal of this paper is to derive a thermodynamically consistent phase-field model for vesicles' motion, shape transformation and their structural interactions under flow conditions in a closed spatial domain using an energy variational method [37, 38]. All the physics that ones are interested in are taken into consideration through definitions of the energy functional and the dissipation functional, together with the kinematic relations of dynamic evolution of model state variables.

In this work, all terms of the energy and dissipation functionals are defined on the bulk region of the domain including cell-cell adhesion and cell-wall interactions. A Lennard-Jones type potential within the framework of phase-field method is derived for the vesicle-vesicle interaction, in which an interacting potential including both repulsive and attractive parts is established with respect to the phase-field order parameter. To consider the cell-wall interaction, the wall is just treated as a new phase-field order parameter or function  $\phi_w(\mathbf{x})$  in the proposed Lennard-Jones type potential. Then, the cell phase-field function  $\phi$  defined on the bulk region of the domain which would be used in the derivation of model governing equations by the energy variational approach [39]. The advantage of doing so is that the variational procedure only needs to consider the bulk unlike previous works [37, 39] where the boundary needs to be considered since the wall effect are included in boundary conditions of the system, which simplifies the model derivation considerably.

Performing variation of the energy and dissipation functionals yields a Cahn-Hilliard-Navier-Stokes (CH-NS) system with Allen-Cahn (AC) general Navier boundary conditions (GNBC) [40, 39]. This is in contrast to most previous works [41, 33, 42] in which boundary effects were rarely derived during the course of model derivation. Dirichlet or Neumann type boundary conditions were simply added to these models at the end to close the governing equations [43, 22, 23, 35, 44].

Moreover, our model accounts for the incompressibility of the fluid, and the local and global inextensibility of the vesicle membrane by introducing two Lagrangian multipliers, hydrostatic pressure  $p$  and surface pressure  $\lambda$  [45] and penalty terms, respectively.

The second goal of this paper is to design an energy stable finite element scheme for solving model governing equations. This scheme preserves a discrete counterpart of the energy dissipation property of the model in numerical solution, which is crucial for long term stability of numerical computation. We note that although this scheme is designed for solving the model equations, it can be easily applied to other CH-NS systems. We apply our model to simulate multiple vesicles interacting with each other and the domain boundaries under flow conditions *in silico*, such as red blood cells passing a branched blood vessel. **elaborate**

Rest of the paper is organized as follows. In Section 2, the thermodynamically consistent model considering cell-cell and cell-wall interaction is derived, the energy dissipation law of the model is given. Then the discrete scheme of the model and the discrete energy law that is consistent with the continuous condition is given in Section 3. Section 4 is used to present results of numerical simulations and compare them with the data collected in laboratory experiments. The conclusion is drawn in Section 5.

## 2. Model Derivation

Derivation of the model in this paper is based on the energy dissipation law which holds ubiquitously in physical systems involving irreversible processes [46, 47, 48, 49, 44]. This law states that for an isothermal and closed system the rate of change of the energy of the system is equal to the dissipation of the energy as follows:

$$\frac{d}{dt}E^{\text{total}} = -\Delta \leq 0, \quad (1)$$

where  $E^{\text{total}}$  is the total energy of the system, which is the sum of the kinetic energy  $\mathcal{K}$  and the Helmholtz free energy  $\mathcal{F}$  of the system, and  $\Delta$  is the rate of energy dissipation, which in fact is entropy production. Eq. (1) can be easily derived via the combination of the First and Second Laws of Thermodynamics. The choices of the total energy functional and the dissipation functional, together with the kinematic (transport) relations of the variables employed in the system, determine all the physical and mechanical considerations and assumptions for the problem [50]. A general technique to determine these relations of variables may be found in [38, 44].

### 2.1. Multi-vesicle interaction System

Energy variational method [37] is adopted for model derivation to ensure the thermodynamics consistency of the derived model. Specifically, the model respects the energy dissipation law given by (1). The model derivation begins with defining functionals of the total energy and dissipation of the system, respectively, and making the kinematic assumptions of the state variables of the system based on physics laws of conservation. We refer the readers to [37, 39, 51] for detailed discussions of this method.

Figure 1 is a schematic showing the setup of the model. Let the problem domain be  $\Omega$ , and its wall boundary be  $\partial\Omega_w$ . For a multi-cell flow system, the dynamic evolution of the  $i^{\text{th}}$  cell (or vesicle) under flow conditions within  $\Omega$  is tracked by the phase-field function  $\phi_i(\mathbf{x}, t)$ . Notice that  $\phi_i(\mathbf{x}, t) \in [-1, 1]$  with  $\phi_i = 1$  for intracellular space and  $\phi_i = -1$  for extracellular space. The membrane of the cell is identified by  $\phi_i(\mathbf{x}, t) = 0$ . We also introduce a phase-field function  $\phi_w(\mathbf{x}) \in [-1, 1]$  to represent the wall boundary of the domain as shown in Fig. 1. This is for considering cell-wall interaction described below.

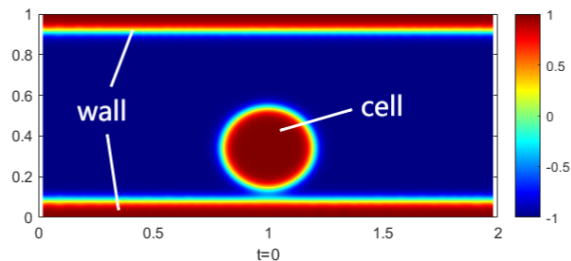


Figure 1: A schematic showing the model setup. Phase-field functions are used to represent the domain wall boundary and the cell interface.

We assume that the dynamical evolution of the phase-field function  $\phi_i$  is a generalized gradient flow, see Eq. (2a). We also utilize the laws of conservation for describing the dynamics of the momentum and the total mass of the system, see Eqs. (2b)-(2c). The cell membrane (interface) is assumed to be inextensible. The equation for local inextensibility of the interface is given by Eq. (2d).

$$\frac{\partial \phi_i}{\partial t} + \nabla \cdot (\mathbf{u} \phi_i) = \nabla \cdot \mathbf{q}_{\phi_i}, \quad (2a)$$

$$\rho \left( \frac{\partial \mathbf{u}}{\partial t} + (\mathbf{u} \cdot \nabla) \mathbf{u} \right) = \nabla \cdot \boldsymbol{\sigma}_\eta + \mathbf{F}_{\phi_1, \phi_2, \dots, \phi_N}, \quad (2b)$$

$$\nabla \cdot \mathbf{u} = 0, \quad (2c)$$

$$(\mathcal{P}_i : \nabla \mathbf{u}) \delta_i = 0 , \quad (2d)$$

where  $\rho$  is the averaged density of the system. In this work,  $\rho$  is assumed to be a constant.  $\mathbf{u}$  is the macroscopic velocity of the system, and  $\boldsymbol{\sigma}_\eta$  is the system's visco-elastic stress to be determined.

The undetermined flux  $\mathbf{q}_{\phi_i}$  in Eq. (2a) will be determined by postulating that  $\phi_i$  is driven by gradients in a chemical potential. This leads to the Cahn-Hilliard equation which ensures conservation of the volume of a cell during its dynamic evolution.  $\mathbf{F}_{\phi_1, \phi_2, \dots, \phi_n}$  in Eq. (2b) is the body force induced by vesicle-fluid interaction and is to be determined as well.

Equation (2d) is the diffuse interface approximation of the local inextensibility of the membrane of the  $i^{th}$  cell with relaxation [39, 43].  $\delta_i = \frac{1}{2}\gamma^2|\nabla\phi_i|^2$  is the surface delta function with the diffuse interface thickness  $\gamma$ .  $\mathcal{P}_i$  is the projection operator, and is defined to be  $(I - \mathbf{n}_{i,m} \otimes \mathbf{n}_{i,m})$ .  $\mathbf{n}_{i,m} = \frac{\nabla\phi_i}{|\nabla\phi_i|}$  is the unit outward normal vector of the interface when it is defined as an implicit surface by the phase-field function. This equation is equivalent to  $\mathcal{P}_i : \nabla \mathbf{u} = 0$  under a sharp interface condition. In phase field frame, this local inextensibility is extended to the whole domain by multiplying a scalar function  $\delta_i$  [37] for the convenience of computation. Following the idea in [43, 39], here we add a relaxation term  $\xi\gamma^2\nabla(\phi_i^2\nabla\lambda_i)$  in Eq. (2d) where  $\xi$  is a parameter independent of  $\gamma$ ,  $\lambda_i$  is a function that measures the interface "pressure" induced by the inextensibility of the membrane of the  $i^{th}$  cell. Thus Eq. (2d) now takes the form:

$$(\mathcal{P}_i : \nabla \mathbf{u}) \delta_i + \xi\gamma^2\nabla(\phi_i^2\nabla\lambda_i) = 0 \quad (3)$$

Eq.(2a)-(2c) and (3) together constitute the governing equations of the system.

The boundary conditions on the top and bottom of the domain, denoted by  $\partial\Omega_w$ , are given as follows:

$$\begin{cases} \mathbf{u} \cdot \mathbf{n} = 0 , \\ \mathbf{u}_\tau \cdot \boldsymbol{\tau}_k = f_{\tau_k} , \\ \frac{\partial\phi_i}{\partial t} + \mathbf{u} \cdot \nabla_\Gamma \phi_i = J_{\Gamma_i} , \\ \mathbf{q}_{\phi_i} \cdot \mathbf{n} = 0 . \end{cases} \quad (4)$$

On the boundary  $\partial\Omega_w$ , an Allen-Cahn (4)<sub>3</sub> type boundary condition is employed for  $\phi_i$ .  $\nabla_\Gamma = \nabla - \mathbf{n}(\mathbf{n} \cdot \nabla)$  is the surface gradient operator, and  $\mathbf{u}_\tau = \mathbf{u} - (\mathbf{u} \cdot \mathbf{n})\mathbf{n}$  is the fluid slip velocity with respect to the wall where  $\boldsymbol{\tau}_i, i = 1, 2$  are the tangential directions of the wall surface.  $\mathbf{n}$  is the unit outward normal vector of the wall.  $f_{\tau_i}$  is the slip velocity of the fluid on the wall along the  $\boldsymbol{\tau}_i$  direction.  $J_\Gamma$  represents the Allen-Cahn type of relaxation on the wall by using the phase-field method, and is to be determined, see [52, 37].

The total energy functional  $E_{total}$  for the multi-cell system is assumed to be the sum of the kinetic energy  $E_{kin}$  in the macroscale, elastic energy  $E_{cell}$  of cell membrane, cell-cell interaction energy  $E_{int}$  and cell-wall adhesion energy  $E_w$  in the microscale. Therefore

$$\begin{aligned} E_{total} &= \underbrace{E_{kin}}_{\text{Macroscale}} + \underbrace{E_{cell} + E_{int} + E_w}_{\text{Microscale}} \quad (5) \\ &= \int_\Omega \left( \frac{1}{2}\rho|\mathbf{u}|^2 \right) d\mathbf{x} + \sum_{i=1}^N \int_\Omega \frac{\hat{\kappa}_B}{2\gamma} \left| \frac{f(\phi_i)}{\gamma} \right|^2 d\mathbf{x} + \sum_{i=1}^N \frac{\mathcal{M}_s}{2} \frac{(S(\phi_i(t)) - S(\phi_i(t=0)))^2}{S(\phi_i(t=0))} \\ &+ \int_\Omega H d\mathbf{x} + \sum_{i=1}^N \int_\Omega f_w(\phi_i) ds . \quad (6) \end{aligned}$$

Here  $\hat{\kappa}_B$  is the bending modulus of the membrane, and  $\gamma$  is the thickness of the diffuse interface. The membrane energy density is given by

$$f(\phi_i) = \frac{\delta G}{\delta \phi_i} = -\gamma^2 \Delta \phi_i + (\phi_i^2 - 1)\phi_i , \quad (7)$$

with

$$G(\phi_i) = \frac{\gamma^2 |\nabla \phi_i|^2}{2} + \frac{(1 - \phi_i^2)^2}{4} . \quad (8)$$

The function  $S(\phi_i) = \int_{\Omega} \frac{G(\phi_i)}{\gamma} dx$  is used to measure the surface area of the cell [43, 22, 37].  $\mathcal{M}_s$  is the penalty constant.

The term  $H$  denotes the interaction energy density induced by the interaction of cells. There are many different ways to define  $H$  [28, 29, 24]. Here we begin with considering mechanical interaction between two cells identified by phase-field functions  $\phi_1$  and  $\phi_2$ , respectively. Recall that  $\phi_i = 1$  represents the intracellular space, and  $\phi_i = -1$  represents the extracellular space of the  $i^{\text{th}}$  cell, respectively. Whether there exists mechanical interaction between the two cells can be determined by measuring the overlapping (i.e., occupying the same physical space) of the membranes of these two cells. The following two functions are introduced to measure the overlapping

$$d_1(\mathbf{x}) = (\phi_1(\mathbf{x}) - 1)(\phi_2(\mathbf{x}) - 1), \quad \mathbf{x} \in \Omega,$$

and

$$d_2(\mathbf{x}) = (\phi_1(\mathbf{x}) + 1)(\phi_2(\mathbf{x}) + 1), \quad \mathbf{x} \in \Omega.$$

It is obvious that  $d_1, d_2 \in [0, 4]$ . From physical point of view, we can regard  $d_1$  as the ‘‘distance’’ in the space of phase-field functions since it reaches maximum when both  $\phi_1$  and  $\phi_2$  equal to -1 which means there is no overlap between the two cells.  $d_1$  reaches minimum when two cells fully overlap, i.e.,  $\phi_1 = \phi_2 = 1$ . Similarly,  $d_2$  could be regarded as the extent of overlapping since it reaches maximum when cells fully overlap, and reaches minimum when there is no overlap. Then we propose the interaction potential  $H$  by a polynomial function of  $d_2$  and  $d_1$ :

$$H = Q(d_2^\alpha + C)d_1^\beta = QC(\phi_1 + 1)^\beta(\phi_2 + 1)^\beta - Q(\phi_1^2 - 1)^\alpha(\phi_2 - 1)^\alpha(\phi_1 + 1)^{\beta-\alpha}(\phi_2 + 1)^{\beta-\alpha}, \quad (9)$$

where  $Q$  and  $C$  are constant that controls the minimum of the interaction energy. The first term of Eq. (9) accounts for the repulsion between the two cells which increase sharply to prevent fully overlapping of the cells, and the second terms is for the attraction between cells which only appears when the cells contact each other, which means the they start to overlap.

In this work, we take  $\alpha = \beta = 2$ . Thus the interaction potential (9) becomes:

$$H = Q_1(\phi_1 + 1)^2(\phi_2 + 1)^2 - Q_2(\phi_1^2 - 1)^2(\phi_2^2 - 1)^2. \quad (10)$$

Now we may consider  $H$  as a 2D function of  $\phi_1$  and  $\phi_2$ , where both  $\phi_1$  and  $\phi_2$  take values between -1 and 1 and their values represent relative position of vesicle 1 and vesicle 2 when they overlap. Also we need to point out that it is because  $H$  is regarded as a 2D function, we need two variables ( $d_1, d_2$ ) or  $(\phi_1, \phi_2)$  to formulate a single-concave potential energy with only one minima in the domain. Figure 2 plots the energy landscape of the interaction potential due to presence of the phases  $\phi_1$  and  $\phi_2$ . The energy is equal to 0 when two phases do not touch or overlap i.e.,  $\phi_1 = \phi_2 = -1$ . When they start to overlap, the energy firstly decreases which means that the attraction force between these two phases dominates. Then the energy goes up which indicates the repulsive force dominates. This prevents the two phases from occupying the same physical space. So the interacting potential energy behaves conceptually similar to a 2D kind of Lennard-Jones potential. We should point out that Eq. (9) or (10) is just constructed to mimic Lennard-Jones type of repulsive-attractive feature. Other formula with similar behavior may be good too. We remark that in [25] a potential of form  $(\phi_1^2 - 1)^2(\phi_2^2 - 1)$  is used, where only attractive feature is included.

More general, the interaction energy in multiple phases case goes:

$$H = \sum_{i=1}^N \sum_{i < j} H_{ij} = \sum_{i=1}^N \sum_{i < j} [Q_1(\phi_i + 1)^2(\phi_j + 1)^2 - Q_2(\phi_i^2 - 1)^2(\phi_j^2 - 1)^2]. \quad (11)$$

For the cell-wall adhesion energy,  $\phi_w$  is defined along the wall with a thickness [25] as shown in Figure 4. Following above interaction potential definition, then the cell-wall interaction energy is defined by setting  $\phi_2 = \phi_w$  in Eq. (10),

$$f_w(\phi_i) = Q_{w_1}(\phi_i + 1)^2(\phi_w + 1)^2 - Q_{w_2}(\phi_i^2 - 1)^2(\phi_w^2 - 1)^2, \quad (12)$$

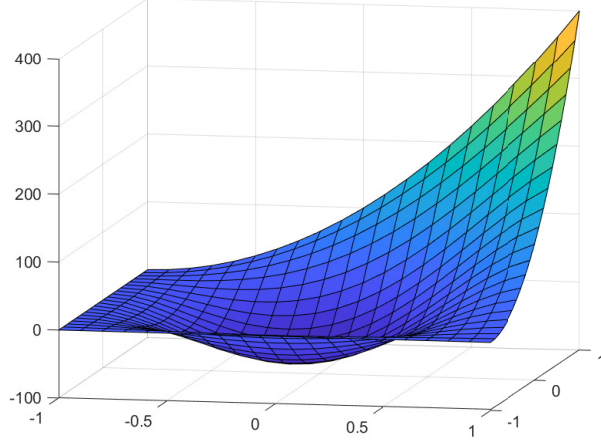


Figure 2: Interaction energy with respect to  $\phi_1$  and  $\phi_2$  with  $Q_1 = 50$ ,  $Q_2 = 400$ .

where  $Q_{w_1}$  is repulsive energy density and  $Q_{w_2}$  is adhesion energy density. Notice that the cell-wall energy  $E_w$  is defined in the bulk not on the boundary. However,  $f_w$  is non-zero only when the two phases overlap which could be regarded as the attraction force is only induced when the vesicle is contacting (or close enough to) the wall.

Then the chemical potential  $\mu_i$  for each phase  $\phi_i$  is defined as follows

$$\mu_i = \frac{\delta E_{cell_i}}{\delta \phi_i} = \frac{\hat{\kappa}_B}{\gamma^3} g(\phi_i) + \frac{\partial H}{\partial \phi_i} + \frac{\mathcal{M}_s}{\gamma} \frac{S(\phi_i) - S(\phi_{i,0})}{S(\phi_{i,0})} f(\phi_i) + \frac{\partial f_w(\phi_i)}{\partial \phi_i}, \quad (13)$$

where  $g(\phi_i) = -\gamma^2 \Delta f(\phi_i) + (3\phi_i^2 - 1)f(\phi_i)$ .

The dissipation functional of the system consists of the dissipation introduced by fluid viscosity, friction near the wall, and interfacial mixing due to the diffuse interface representation [39]:

$$\begin{aligned} \Delta = & \int_{\Omega} 2\eta |\mathbf{D}_{\eta}|^2 d\mathbf{x} + \sum_{i=1}^N \int_{\Omega} \frac{1}{M_{\phi}} |q_{\phi_i}|^2 d\mathbf{x} + \int_{\partial\Omega_w} \beta_s |\mathbf{u}_{\tau}|^2 ds \\ & + \sum_{i=1}^N \left( \int_{\partial\Omega_w} \kappa_{\Gamma} |J_{\Gamma_i}|^2 ds + \int_{\partial\Omega_w} \xi |\gamma \phi_i \nabla \lambda_i|^2 ds \right), \end{aligned} \quad (14)$$

where  $\mathbf{D}_{\eta} = \frac{\nabla \mathbf{u} + (\nabla \mathbf{u})^T}{2}$ ,  $\eta$  is the viscosity of fluid mixture,  $\beta_s$  is wall fraction,  $M_{\phi}$  and  $\kappa_{\Gamma}$  are the mobility of phase in the bulk and boundary. We note that in general, the viscosity  $\eta$  could be a function of all phases  $\phi_i$

$$\eta = \eta(\phi_w, \phi_1, \dots, \phi_n). \quad (15)$$

The specific forms of the flux and stress functions in the kinematic equations (2)-(4) are obtained by taking the time derivative of the total energy functional and comparing with the defined dissipation functional. Then the time derivative of the total energy goes:

$$\frac{dE_{total}}{dt} = \frac{d}{dt} E_{kin} + \frac{d}{dt} E_{cell} + \frac{d}{dt} E_w \quad (16)$$

$$\equiv I_1 + I_2 + I_3. \quad (17)$$

Taking the time derivative of  $E_{kin}$ , together with the conservation law of momentum (2)<sub>2</sub>, incompressibility of the fluid (2)<sub>3</sub> and inextensibility of the membrane (2)<sub>4</sub> yields

$$\begin{aligned}
I_1 &= \frac{d}{dt} \int_{\Omega} \frac{\rho |\mathbf{u}|^2}{2} d\mathbf{x} \\
&= \int_{\Omega} \frac{1}{2} \frac{\partial \rho}{\partial t} |\mathbf{u}|^2 d\mathbf{x} + \int_{\Omega} \rho \frac{\partial \mathbf{u}}{\partial t} \cdot \mathbf{u} d\mathbf{x} \\
&= \int_{\Omega} \frac{1}{2} \frac{\partial \rho}{\partial t} |\mathbf{u}|^2 d\mathbf{x} + \int_{\Omega} \rho \frac{d\mathbf{u}}{dt} \cdot \mathbf{u} d\mathbf{x} - \int_{\Omega} (\rho \mathbf{u} \cdot \nabla \mathbf{u}) \cdot \mathbf{u} d\mathbf{x} \\
&= \int_{\Omega} \frac{1}{2} \frac{\partial \rho}{\partial t} |\mathbf{u}|^2 d\mathbf{x} + \int_{\Omega} \rho \frac{d\mathbf{u}}{dt} \cdot \mathbf{u} d\mathbf{x} + \int_{\Omega} \nabla \cdot (\rho \mathbf{u}) \frac{|\mathbf{u}|^2}{2} d\mathbf{x} \\
&= \int_{\Omega} (\nabla \cdot \boldsymbol{\sigma}_{\eta}) \cdot \mathbf{u} d\mathbf{x} + \int_{\Omega} \mathbf{F} \cdot \mathbf{u} d\mathbf{x} + \sum_{i=1}^N \int_{\Omega} \lambda_i \delta_i \mathcal{P}_i : \nabla \mathbf{u} d\mathbf{x} + \sum_{i=1}^N \int_{\Omega} \xi \gamma^2 \lambda_i \nabla \cdot (\phi_i^2 \nabla \lambda_i) d\mathbf{x} - \int_{\Omega} p I : \nabla \mathbf{u} d\mathbf{x} \\
&= - \int_{\Omega} ((\boldsymbol{\sigma}_{\eta} + pI) : \nabla \mathbf{u}) d\mathbf{x} + \int_{\Omega} \mathbf{F} \cdot \mathbf{u} d\mathbf{x} - \sum_{i=1}^N \int_{\Omega} \nabla \cdot (\lambda_i \delta_i \mathcal{P}_i) \cdot \mathbf{u} d\mathbf{x} \\
&\quad - \sum_{i=1}^N \int_{\Omega} \xi \gamma^2 \phi_i^2 (\nabla \lambda_i)^2 d\mathbf{x} + \int_{\partial \Omega_w} ((\boldsymbol{\sigma}_{\eta} + \sum_{i=1}^N \lambda_i \delta_i \mathcal{P}_i) \cdot \mathbf{n}) \cdot \mathbf{u}_{\tau} dS, \tag{18}
\end{aligned}$$

where the slip boundary condition is used. Here the pressure  $p$  is a Lagrangian multiplier and is introduced to ensure the incompressibility of the fluid.

Taking the time derivative of  $E_{cell}$  together with the conservation of each phase (2)<sub>1</sub> yields

$$\begin{aligned}
I_2 &= \frac{d}{dt} \int_{\Omega} \frac{\hat{\kappa}_B}{2\gamma} \sum_{i=1}^N \left| \frac{f(\phi_i)}{\gamma} \right|^2 d\mathbf{x} + \frac{d}{dt} \int_{\Omega} H d\mathbf{x} + \sum_{i=1}^N \frac{d}{dt} \frac{\mathcal{M}_s}{2} \frac{(S(\phi_i) - S(\phi_{i,0}))^2}{S(\phi_{i,0})} \\
&= \int_{\Omega} \frac{\hat{\kappa}_B}{\gamma} \sum_{i=1}^N \frac{f_i}{\gamma^2} \frac{\partial f_i}{\partial t} d\mathbf{x} + \int_{\Omega} \sum_{i=1}^N \frac{\partial H}{\partial \phi_i} \frac{\partial \phi_i}{\partial t} d\mathbf{x} + \sum_{i=1}^N \frac{d}{dt} \frac{\mathcal{M}_s}{2} \frac{(S(\phi_i) - S(\phi_{i,0}))^2}{S(\phi_{i,0})} \\
&= \int_{\Omega} \frac{\hat{\kappa}_B}{\gamma} \sum_{i=1}^N \frac{f_i}{\gamma^2} \left( -\gamma^2 \Delta \left( \frac{\partial \phi_i}{\partial t} \right) + (3\phi_i^2 - 1) \frac{\partial \phi_i}{\partial t} \right) d\mathbf{x} + \int_{\Omega} \sum_{i=1}^N \frac{\partial H}{\partial \phi_i} \frac{\partial \phi_i}{\partial t} d\mathbf{x} \\
&\quad + \sum_{i=1}^N \frac{d}{dt} \frac{\mathcal{M}_s}{2} \frac{(S(\phi_i) - S(\phi_{i,0}))^2}{S(\phi_{i,0})} \\
&= \int_{\Omega} \frac{\hat{\kappa}_B}{\gamma^3} \sum_{i=1}^N \left( -\gamma^2 \Delta f_i + (3\phi_i^2 - 1) f_i + \frac{\partial H}{\partial \phi_i} + \frac{\mathcal{M}_s}{\gamma} \frac{S(\phi_i) - S(\phi_{i,0})}{S(\phi_{i,0})} f(\phi_i) \right) \frac{\partial \phi_i}{\partial t} d\mathbf{x} \\
&\quad - \int_{\partial \Omega_w} \frac{\hat{\kappa}_B}{\gamma} \sum_{i=1}^N f_i \frac{\partial}{\partial t} (\partial_n \phi_i) ds + \int_{\partial \Omega_w} \frac{\hat{\kappa}_B}{\gamma} \sum_{i=1}^N \partial_n f_i \frac{\partial \phi_i}{\partial t} ds + \sum_{i=1}^N \int_{\partial \Omega_w} \mathcal{M}_s \frac{S(\phi_i) - S(\phi_{i,0})}{S(\phi_{i,0})} \gamma \partial_n \phi_i \frac{\partial \phi_i}{\partial t} ds \\
&= \sum_{i=1}^N \left( \int_{\Omega} \mu_i \frac{\partial \phi_i}{\partial t} d\mathbf{x} + \int_{\partial \Omega_w} \frac{\hat{\kappa}_B}{\gamma} f_i \frac{\partial}{\partial t} (\partial_n \phi_i) ds + \int_{\partial \Omega_w} \mathcal{M}_s \frac{S(\phi_i) - S(\phi_{i,0})}{S(\phi_{i,0})} \gamma \partial_n \phi_i \frac{\partial \phi_i}{\partial t} ds \right) \\
&= \sum_{i=1}^N \left( \int_{\Omega} \mu_i \nabla \cdot \mathbf{q}_{\phi_i} d\mathbf{x} - \int_{\Omega} \mu_i \mathbf{u} \cdot \nabla \phi_i d\mathbf{x} + \int_{\partial \Omega_w} \frac{\hat{\kappa}_B}{\gamma} \partial_n f_i \frac{\partial \phi_i}{\partial t} ds + \int_{\partial \Omega_w} \mathcal{M}_s \frac{S(\phi_i) - S(\phi_{i,0})}{S(\phi_{i,0})} \gamma \partial_n \phi_i \frac{\partial \phi_i}{\partial t} ds \right) \\
&= \sum_{i=1}^N \left( - \int_{\Omega} \mathbf{q}_{\phi_i} \cdot \nabla \mu_i d\mathbf{x} - \int_{\Omega} \mu_i \mathbf{u} \cdot \nabla \phi_i d\mathbf{x} + \int_{\partial \Omega_w} \frac{\hat{\kappa}_B}{\gamma} \partial_n f_i \frac{\partial \phi_i}{\partial t} ds \right)
\end{aligned}$$

$$+ \int_{\partial\Omega_w} \mathcal{M}_s \frac{S(\phi_i) - S(\phi_{i,0})}{S(\phi_{i,0})} \gamma \partial_n \phi_i \frac{\partial \phi_i}{\partial t} ds \Big), \quad (19)$$

where the Allan-Cahn boundary condition (4)<sub>3</sub> for each phase is used.

Computing  $\frac{d}{dt} E_w$  yields

$$I_3 = \sum_{i=1}^N \left( \int_{\partial\Omega} \frac{\partial f_w(\phi_i)}{\partial \phi_i} \frac{\partial \phi_i}{\partial t} ds \right). \quad (20)$$

By combining Eqs. (18), (19) and (20), we have:

$$\begin{aligned} \frac{d}{dt} E_{total} &= - \int_{\Omega} ((\boldsymbol{\sigma}_\eta + pI) : \nabla \mathbf{u}) d\mathbf{x} + \int_{\Omega} (\mathbf{F} - \sum_{i=1}^N \mu_i \nabla \phi_i - \sum_{i=1}^N \nabla \cdot (\lambda_i \delta_i \mathcal{P}_i)) \cdot \mathbf{u} d\mathbf{x} \\ &\quad - \sum_{i=1}^N \int_{\Omega} q_{\phi_i} \cdot \nabla \mu_i d\mathbf{x} + \sum_{i=1}^N \int_{\Omega} \xi \gamma^2 \phi_i^2 (\nabla \lambda_i)^2 d\mathbf{x} + \int_{\partial\Omega_w} ((\boldsymbol{\sigma}_\eta + \sum_{i=1}^N \lambda_i \delta_i \mathcal{P}_i) \cdot \mathbf{n}) \cdot \mathbf{u}_\tau ds + \sum_{i=1}^N \int_{\partial\Omega_s} \hat{L}_i \frac{\partial \phi_i}{\partial t} ds \\ &= - \int_{\Omega} ((\boldsymbol{\sigma}_\eta + pI) : \nabla \mathbf{u}) d\mathbf{x} + \int_{\Omega} (\mathbf{F} - \sum_{i=1}^N \mu_i \nabla \phi_i - \sum_{i=1}^N \nabla \cdot (\lambda_i \delta_i \mathcal{P}_i)) \cdot \mathbf{u} d\mathbf{x} \\ &\quad - \sum_{i=1}^N \int_{\Omega} q_{\phi_i} \cdot \nabla \mu_i d\mathbf{x} + \sum_{i=1}^N \int_{\Omega} \xi \gamma^2 \phi_i^2 (\nabla \lambda_i)^2 d\mathbf{x} + \int_{\partial\Omega_w} ((\boldsymbol{\sigma}_\eta + \sum_{i=1}^N \lambda_i \delta_i \mathcal{P}_i) \cdot \mathbf{n}) \cdot \mathbf{u}_\tau ds \\ &\quad + \sum_{i=1}^N \int_{\partial\Omega_s} \hat{L}_i (-\mathbf{u} \cdot \nabla_\Gamma \phi_i + J_{\Gamma_i}) ds \\ &= - \int_{\Omega} ((\boldsymbol{\sigma}_\eta + pI) : \nabla \mathbf{u}) d\mathbf{x} + \int_{\Omega} (\mathbf{F} - \sum_{i=1}^N \mu_i \nabla \phi_i - \sum_{i=1}^N \nabla \cdot (\lambda_i \delta_i \mathcal{P}_i)) \cdot \mathbf{u} d\mathbf{x} \\ &\quad - \sum_{i=1}^N \int_{\Omega} q_{\phi_i} \cdot \nabla \mu_i d\mathbf{x} + \sum_{i=1}^N \int_{\Omega} \xi \gamma^2 \phi_i^2 (\nabla \lambda_i)^2 d\mathbf{x} + \int_{\partial\Omega_w} ((\boldsymbol{\sigma}_\eta + \sum_{i=1}^N \lambda_i \delta_i \mathcal{P}_i) \cdot \mathbf{n} - \sum_{i=1}^N \hat{L}_i \nabla_\Gamma \phi_i) \cdot \mathbf{u}_\tau ds \\ &\quad + \sum_{i=1}^N \int_{\partial\Omega_w} \hat{L}_i J_{\Gamma_i} ds, \end{aligned} \quad (21)$$

where  $\hat{L}_i = \frac{\hat{\kappa}_B}{\gamma} \partial_n f_i + \mathcal{M}_s \frac{S(\phi_i) - S(\phi_{i,0})}{S(\phi_{i,0})} \gamma \partial_n \phi_i$ .

To close the system, we use the energy dissipation law [49, 37, 53]

$$\frac{dE}{dt} = -\Delta, \quad (22)$$

which states that the rate of changing total energy of the system is induced by the dissipation. Comparing Eq. (21) with predefined dissipation functional in Eq. (14) gives rise to

$$\begin{cases} \boldsymbol{\sigma}_\eta = 2\eta \mathbf{D}_\eta - pI, & \text{in } \Omega, \\ q_{\phi_j} = M_{\phi_j} \nabla \mu_j, & \text{in } \Omega, \\ \mathbf{F} = \sum_{i=1}^N (\mu_i \nabla \phi_i + \nabla \cdot (\lambda_i \delta_i \mathcal{P}_i)), & \text{in } \Omega, \\ J_{\Gamma_i} = -\kappa_{\Gamma_i}^{-1} \hat{L}_i, & \text{on } \partial\Omega_w, \\ u_{\tau_j} = \beta_s^{-1} (-\mathbf{n} \cdot (\boldsymbol{\sigma}_\eta + \sum_{i=1}^N \lambda_i \delta_i \mathcal{P}_i) \cdot \boldsymbol{\tau}_j) + \sum_{i=1}^N \hat{L}_i \partial_{\tau_j} \phi_i, \quad j = 1, 2, & \text{on } \partial\Omega_w. \end{cases} \quad (23)$$

To this end, the proposed multi-cellular interaction model is composed of the following equations:



$$\begin{cases} \frac{\partial \phi_i}{\partial t} + \nabla \cdot (\mathbf{u} \phi_i) = M_{\phi_i} \Delta \mu_i , \\ \mu_i = \frac{\hat{\kappa}_B}{\gamma^3} g(\phi_i) + \frac{\partial H}{\partial \phi_i} + \frac{M_s}{\gamma} \frac{S(\phi_i) - S(\phi_{i,0})}{S(\phi_{i,0})} f(\phi_i) + \frac{\partial f_w(\phi_i)}{\partial \phi_i} , \\ g(\phi_i) = -\gamma^2 \Delta f_i + (3\phi_i^2 - 1) f(\phi_i) , \\ f(\phi_i) = -\gamma^2 \Delta \phi_i + (\phi_i^2 - 1) \phi_i , \\ \rho \left( \frac{\partial \mathbf{u}}{\partial t} + (\mathbf{u} \cdot \nabla) \mathbf{u} \right) + \nabla p = \nabla \cdot (2\eta \mathbf{D}_\eta) + \sum_{j=1}^i (\mu_j \nabla \phi_j + \nabla \cdot (\lambda_j \delta_j \mathcal{P}_j)) , \\ \nabla \cdot \mathbf{u} = 0 , \\ \delta_i(\mathcal{P}_i : \nabla \mathbf{u}) + \xi \gamma^2 \nabla \cdot (\phi_i^2 \nabla \lambda_i) = 0 , \end{cases} \quad (24)$$

with the boundary conditions on  $\partial\Omega_w$

$$\begin{cases} \mathbf{u} \cdot \mathbf{n} = 0 , \\ -\beta_s u_{\tau_j} = (\mathbf{n} \cdot (\boldsymbol{\sigma}_\eta + \sum_{i=1}^N \lambda_i \delta_i \mathcal{P}_i) \cdot \boldsymbol{\tau}_j) - \sum_{i=1}^N \hat{L}_i \partial_{\tau_j} \phi_i , \quad j = 1, 2, \\ f_i = 0 , \\ \kappa_{\Gamma_i} \left( \frac{\partial \phi_i}{\partial t} + \mathbf{u} \cdot \nabla_{\Gamma} \phi_i \right) = -\hat{L}_i , \\ \hat{L}_i = \frac{\hat{\kappa}_B}{\gamma} \partial_n f_i + \mathcal{M}_s \frac{S(\phi_i) - S(\phi_{i,0})}{S(\phi_{i,0})} \gamma \partial_n \phi_i , \\ \partial_n \mu_i = 0 . \end{cases} \quad (25)$$

## 2.2. Dimensionless governing equations

The viscosity, length, velocity, time, bulk and boundary chemical potentials in the equations are scaled by their corresponding characteristic values  $\eta_0$ ,  $L$ ,  $U$ ,  $\frac{L}{U}$ ,  $\frac{\eta_0 U}{L}$  and  $\eta_0 U$ , respectively. Write  $Q_{w_1}, Q_{w_2}, Q_1, Q_2$  into  $Q_0 q_{w_1}, Q_0 q_{w_2}, Q_0 q_1, Q_0 q_2$ , where  $Q_0$  is the character energy density. The governing equation of the system can be rewritten as

$$\begin{cases} Re \left( \frac{\partial \mathbf{u}}{\partial t} + (\mathbf{u} \cdot \nabla) \mathbf{u} \right) + \nabla P = \nabla \cdot (2\eta \mathbf{D}) + \sum_i \mu_i \nabla \phi_i + \sum_i \nabla \cdot (\lambda_i \delta_{\epsilon_i} \mathcal{P}_i) , & \text{in } \Omega , \\ \nabla \cdot \mathbf{u} = 0 , & \text{in } \Omega , \\ \frac{\partial \phi_i}{\partial t} + \mathbf{u} \cdot \nabla \phi_i = -\mathcal{M} \Delta \mu_i , & \text{in } \Omega , \\ \mu_i = \kappa_B g(\phi_i) + \mathcal{M}_s \frac{S(\phi_i) - S(\phi_{i,0})}{S(\phi_{i,0})} f_i + \alpha \frac{\partial H}{\partial \phi_i} + \alpha \frac{\partial f_w(\phi_i)}{\partial \phi_i} , & \text{in } \Omega , \\ f_i = -\epsilon \Delta \phi_i + \frac{(\phi_i^2 - 1)}{\epsilon} \phi_i , \quad g(\phi_i) = -\Delta f_i + \frac{1}{\epsilon^2} (3\phi_i^2 - 1) f_i , & \text{in } \Omega , \\ \delta_{\epsilon_i}(\mathcal{P}_i : \nabla \mathbf{u}) + \xi \epsilon^2 \nabla \cdot (\phi_i^2 \nabla \lambda_i) = 0 , & \text{in } \Omega , \end{cases} \quad (26)$$

with the boundary conditions

$$\begin{cases} \kappa \dot{\phi}_i + L(\phi_i) = 0 , & \text{on } \partial\Omega_w , \\ L(\phi_i) = \kappa_B \partial_n f(\phi_i) + \epsilon \mathcal{M}_s \frac{S(\phi_i) - S(\phi_{i,0})}{S(\phi_{i,0})} \partial_n \phi_i , & \text{on } \partial\Omega_w , \\ -l_s^{-1} u_{\tau_i} = \boldsymbol{\tau}_i \cdot (2\eta \mathbf{D}_\eta + \sum_i \lambda_i \delta_{\epsilon_i} \mathcal{P}_i) \cdot \mathbf{n} - \sum_i L(\phi_i) \partial_{\tau_i} \phi_i , \quad i = 1, 2, & \text{on } \partial\Omega_w , \\ f_i = 0 , & \text{on } \partial\Omega_w , \\ \partial_n \mu_i = 0 , & \text{on } \partial\Omega_w , \end{cases} \quad (27)$$

where  $S(\phi_i) = \int_{\Omega} \frac{\epsilon}{2} |\nabla \phi_i|^2 + \frac{1}{4\epsilon} (\phi_i^2 - 1)^2 d\mathbf{x}$  and  $\delta_{\epsilon_i} = \frac{1}{2} \epsilon^2 |\nabla \phi_i|^2$ .

The dimensionless constants appeared in Eqs. (26)-(27) are given by  $\epsilon = \frac{\gamma}{L}$ ,  $Re = \frac{\rho_0 U L}{\eta_0}$ ,  $\mathcal{M} = \frac{M_\phi \eta_0}{L^2}$ ,  $\kappa_B = \frac{\hat{\kappa}_B}{L^2 \eta_0 U}$ ,  $k = \frac{\hat{\kappa}_B}{\eta_0 L}$ ,  $l_s = \frac{\eta_0}{\beta_s L}$ ,  $\alpha = \frac{Q_0}{\eta_0 U}$ ,  $\mathcal{M}_s = \frac{M_s}{\eta_0 U}$ .

If we define the Sobolev spaces as follows [54, 37]

$$\mathbf{W}^{1,3} = (W^{1,3})^2 , \quad (28)$$

$$\mathbf{W}_N^{1,\frac{3}{2}} = (W^{1,\frac{3}{2}})^N, \quad (29)$$

$$\mathbf{W}_N^{1,3} = (W^{1,3})^N, \quad (30)$$

$$\mathbf{W}_N^{1,\frac{3}{2}}(\Omega) = \{\Lambda = (\lambda_1, \lambda_2, \dots, \lambda_N)^T\}, \quad (31)$$

$$\mathbf{W}^{1,3}(\Omega) = \{\mathbf{u} = (u_x, u_y)^T \in \mathbf{W}^{1,3} | \mathbf{u} \cdot \mathbf{n} = 0, \text{ on } \partial\Omega_w\}, \quad (32)$$

$$\mathbf{W}_\Phi^{1,3}(\Omega) = \{\Phi = (\phi_1, \phi_2, \dots, \phi_N)^T \in \mathbf{W}_N^{1,3} | -1 \leq \phi_i \leq 1, i = 1, 2, \dots, N, \text{ in } \Omega\}, \quad (33)$$

$$\mathbf{W}_U^{1,3}(\Omega) = \{U = (\mu_1, \mu_2, \dots, \mu_N)^T \in \mathbf{W}_N^{1,3} | \partial_n \mu_i = 0, i = 1, 2, \dots, N, \text{ on } \partial\Omega_w\}, \quad (34)$$

$$\mathbf{W}_F^{1,3}(\Omega) = \{F = (f_1, f_2, \dots, f_N)^T \in \mathbf{W}_N^{1,3} | f_i = 0, i = 1, 2, \dots, N, \text{ on } \partial\Omega_w\}, \quad (35)$$

$$\mathbf{W}_b = \mathbf{W}_\Phi^{1,3}(\Omega) \times \mathbf{W}_F^{1,3}(\Omega) \times \mathbf{W}_U^{1,3}(\Omega) \times \mathbf{W}_N^{1,\frac{3}{2}}(\Omega) \times W^{1,\frac{3}{2}}(\Omega) \times \mathbf{W}^{1,3}(\Omega), \quad (36)$$

and let  $\|\cdot\| = \left(\int_\Omega |\cdot|^2 d\mathbf{x}\right)^{\frac{1}{2}}$  and  $\|\cdot\|_w = \left(\int_{\partial\Omega_w} |\cdot|^2 ds\right)^{\frac{1}{2}}$  denote the  $L^2$  norm defined in the domain and on the domain boundary respectively, then the system (26)-(27) satisfies the following energy law.

**Theorem 2.1.** *If  $(\Phi, F, U, \lambda, P, \mathbf{u}) \in \mathbf{W}_b$  are smooth solutions of the above system (26)-(27), then the following energy law is satisfied:*

$$\begin{aligned} \frac{d}{dt} \mathcal{E}_{total} &= \frac{d}{dt} (\mathcal{E}_{kin} + \mathcal{E}_{cell} + \mathcal{E}_w) \\ &= \frac{1}{Re} \left( -2\|\eta^{1/2} \mathbf{D}_\eta\|^2 - \mathcal{M} \sum_i \|\nabla \mu_i\|^2 - \xi \sum_i \|\epsilon \phi_i \nabla \lambda_i\|^2 - \kappa \sum_i \|\dot{\phi}_i\|_w^2 - \|l_s^{-1/2} \mathbf{u}_\tau\|_w^2 \right), \end{aligned} \quad (37)$$

where  $\mathcal{E}_{total} = \mathcal{E}_{kin} + \mathcal{E}_{cell} + \mathcal{E}_w$ ,  $\mathcal{E}_{kin} = \frac{1}{2} \int_\Omega |\mathbf{u}|^2 d\mathbf{x}$ ,  $\mathcal{E}_{cell} = \frac{\kappa_B}{2Re\epsilon} \sum_i \int_\Omega |f_i|^2 d\mathbf{x} + \mathcal{M}_s \sum_i \frac{(S(\phi_i) - S(\phi_{i,0}))^2}{2ReS(\phi_{i,0})} + \frac{\alpha}{Re} \int_\Omega H d\mathbf{x}$  and  $\mathcal{E}_w = \frac{\alpha}{Re} \sum_i \int_\Omega f_w(\phi_i) d\mathbf{x}$ .

**Proof:** Multiplying the first equation in Eq. (26) with  $\mathbf{u}$  and integration by parts yield

$$\begin{aligned} \frac{d}{dt} \mathcal{E}_{kin} &= \frac{1}{Re} \left\{ - \int_\Omega 2\eta |\mathbf{D}_\eta|^2 d\mathbf{x} + \int_{\partial\Omega_w} (\boldsymbol{\sigma}_\eta \cdot \mathbf{n}) \cdot \mathbf{u}_\tau ds + \sum_i \int_\Omega \mu_i \nabla \phi_i \cdot \mathbf{u} d\mathbf{x} - \sum_i \int_\Omega \lambda_i \delta_{\epsilon_i} \mathcal{P}_i : \nabla \mathbf{u} d\mathbf{x} \right. \\ &\quad \left. + \sum_i \int_{\partial\Omega_w} (\lambda_i \delta_{\epsilon_i} \mathcal{P}_i \cdot \mathbf{n}) \cdot \mathbf{u}_\tau ds \right\} \\ &= \frac{1}{Re} \left\{ - \int_\Omega 2\eta |\mathbf{D}_\eta|^2 d\mathbf{x} - \sum_i \int_\Omega \lambda_i \delta_{\epsilon_i} \mathcal{P}_i : \nabla \mathbf{u} d\mathbf{x} - l_s^{-1} \int_{\partial\Omega_w} |\mathbf{u}_\tau|^2 ds \right. \\ &\quad \left. + \sum_i \int_{\partial\Omega_w} L(\phi_i) \partial_\tau \phi \cdot \mathbf{u}_\tau ds + \sum_i \int_\Omega \mu_i \nabla \phi_i \cdot \mathbf{u} d\mathbf{x}, \right\} \end{aligned} \quad (38)$$

where the slip boundary condition in Eq. (27) is applied.

Taking the inner product of the third equation in Eq. (26) with  $\frac{\mu_i}{Re}$  and summing up with respect to  $i$  result in

$$\frac{1}{Re} \sum_i \int_\Omega \frac{\partial \phi_i}{\partial t} \mu_i d\mathbf{x} + \frac{1}{Re} \sum_i \int_\Omega \mathbf{u} \cdot \nabla \phi_i \mu_i d\mathbf{x} = -\frac{1}{Re} \mathcal{M} \sum_i \int_\Omega |\nabla \mu_i|^2 d\mathbf{x}, \quad (39)$$

where  $\partial_n \mu_i = 0$  is considered here.

Multiplying the fourth equation in Eq. (26) with  $\frac{1}{Re} \frac{\partial \phi_i}{\partial t}$  and integration by parts give rise to

$$\begin{aligned}
& \frac{1}{Re} \sum_i \int_{\Omega} \mu \frac{\partial \phi_i}{\partial t} d\mathbf{x} \\
&= \frac{1}{Re} \sum_i \left\{ \kappa_B \int_{\Omega} g_i \frac{\partial \phi_i}{\partial t} d\mathbf{x} + \mathcal{M}_s \frac{S(\phi_i) - S(\phi_{i,0})}{S(\phi_{i,0})} \int_{\Omega} f_i \frac{\partial \phi_i}{\partial t} d\mathbf{x} + \alpha \int_{\Omega} \frac{\partial H}{\partial \phi_i} \frac{\partial \phi_i}{\partial t} d\mathbf{x} + \alpha \int_{\Omega} \frac{f_w(\phi_i)}{\partial \phi_i} \frac{\partial \phi_i}{\partial t} d\mathbf{x} \right\} \\
&= \frac{\kappa_B}{Re} \sum_i \int_{\Omega} f_i \frac{\partial}{\partial t} \left( -\Delta \phi_i + \frac{1}{\epsilon^2} (\phi_i^3 - \phi_i) \right) d\mathbf{x} - \frac{\kappa_B}{Re} \sum_i \int_{\partial\Omega_w} \partial_n f_i \frac{\partial \phi_i}{\partial t} ds + \mathcal{M}_s \sum_i \frac{d}{dt} \left( \frac{(S(\phi_i) - S(\phi_{i,0}))^2}{2ReS(\phi_{i,0})} \right) \\
&\quad - \mathcal{M}_s \sum_i \left( \frac{S(\phi_i) - S(\phi_{i,0})}{ReS(\phi_{i,0})} \right) \int_{\partial\Omega_w} \epsilon \partial_n \phi_i \frac{\partial \phi_i}{\partial t} ds + \frac{\alpha}{Re} \sum_i \int_{\Omega} \frac{\partial f_w(\phi_i)}{\partial \phi_i} \frac{\partial \phi_i}{\partial t} d\mathbf{x} + \frac{\alpha}{Re} \sum_i \int_{\Omega} \frac{\partial H}{\partial \phi_i} \frac{\partial \phi_i}{\partial t} d\mathbf{x} \\
&= \frac{d}{dt} \left( \kappa_B \sum_i \int_{\Omega} \frac{|f_i|^2}{2Re\epsilon} d\mathbf{x} \right) + \mathcal{M}_s \frac{d}{dt} \left( \sum_i \frac{(S(\phi_i) - S(\phi_{i,0}))^2}{2ReS(\phi_{i,0})} \right) + \frac{\alpha}{Re} \frac{d}{dt} \sum_i \int_{\Omega} f_w(\phi_i) d\mathbf{x} + \frac{\alpha}{Re} \frac{d}{dt} \int_{\Omega} H d\mathbf{x} \\
&\quad - \sum_i \int_{\partial\Omega_w} \frac{L(\phi_i)}{Re} \frac{\partial \phi_i}{\partial t} ds \\
&= \frac{d}{dt} (\mathcal{E}_{cell} + \mathcal{E}_w) - \int_{\partial\Omega_w} \frac{L(\phi)}{Re} \frac{\partial \phi}{\partial t} ds,
\end{aligned} \tag{40}$$

where the definitions of  $f(\phi)$ ,  $g(\phi)$  and the boundary conditions of  $\phi$  and  $f$  are utilized.

Multiplying the last equations with  $\frac{\lambda_i}{Re}$  and integration by parts and sum up by  $i$  leads to

$$\frac{1}{Re} \sum_i \int_{\Omega} (\lambda_i \delta_{\epsilon_i} \mathcal{P}_i) : \nabla \mathbf{u} d\mathbf{x} - \frac{1}{Re} \sum_i \int_{\Omega} \xi \epsilon^2 \phi_i^2 (\nabla \lambda_i)^2 d\mathbf{x} = 0. \tag{41}$$

Finally, the energy dissipation law (37) is obtained by combining Eqs. (38), (39), (40) and (41) considering the boundary conditions in (27).  $\blacksquare$

### 3. Numerical Scheme and Discrete Energy Law

In this section, an energy stable temporal discretization scheme is first proposed for the multi-cellular system (26)-(27). Then a  $C^0$  finite element method is used for spacial discretization to obtain the fully discrete scheme.

#### 3.1. Time-discrete primitive method

The mid-point method is used for the temporal discretization of Eqs. (26)-(27). Let  $\Delta t$  denote the time step size,  $(\cdot)^{n+1}$  and  $(\cdot)^n$  denote the values of the variables at times  $(n+1)\Delta t$  and  $n\Delta t$ , respectively. The semi-discrete in time scheme to solve Eq. (26) is as follows:

$$\left\{ \begin{array}{l}
\frac{\mathbf{u}^{n+1} - \mathbf{u}^n}{\Delta t} + (\mathbf{u}^{n+\frac{1}{2}} \cdot \nabla) \mathbf{u}^{n+\frac{1}{2}} + \frac{1}{Re} \nabla P^{n+\frac{1}{2}} = \frac{1}{Re} \nabla \cdot (\eta^n (\nabla \mathbf{u}^{n+\frac{1}{2}} + (\nabla \mathbf{u}^{n+\frac{1}{2}})^T)) \\
\quad + \frac{1}{Re} \sum_i \mu_i^{n+\frac{1}{2}} \nabla \phi_i^{n+\frac{1}{2}} + \sum_i \frac{1}{Re} \nabla \cdot \left( \lambda_i^{n+\frac{1}{2}} \mathcal{P}_i^n \delta_{\epsilon_i} \right), \\
\nabla \cdot \mathbf{u}^{n+\frac{1}{2}} = 0, \\
\frac{\phi_i^{n+1} - \phi_i^n}{\Delta t} + (\mathbf{u}^{n+\frac{1}{2}} \cdot \nabla) \phi_i^{n+\frac{1}{2}} = -\mathcal{M} \Delta \mu_i^{n+\frac{1}{2}}, \\
\mu_i^{n+\frac{1}{2}} = \kappa_B g(\phi_i^{n+1}, \phi_i^n) + \mathcal{M}_s \frac{(S(\phi_i^{n+\frac{1}{2}}) - S(\phi_{0_i}))}{S(\phi_{0_i})} f(\phi_i^{n+1}, \phi_i^n) \\
\quad + \alpha \frac{H_i^{n+1} - H_i^n}{\phi_i^{n+1} - \phi_i^n} + \alpha \frac{f_w(\phi_i^{n+1}) - f_w(\phi_i^n)}{\phi_i^{n+1} - \phi_i^n}, \\
f_i^{n+\frac{1}{2}} = -\epsilon \Delta \phi_i^{n+\frac{1}{2}} + \frac{1}{\epsilon} ((\phi_i^{n+\frac{1}{2}})^2 - 1) \phi_i^{n+\frac{1}{2}}, \\
\delta_{\epsilon_i} \mathcal{P}_i^n : \nabla \mathbf{u}^{n+\frac{1}{2}} + \xi \epsilon^2 \nabla \cdot ((\phi_i^n)^2 \nabla \lambda_i^{n+\frac{1}{2}}) = 0,
\end{array} \right. \tag{42}$$

with boundary conditions on  $\partial\Omega_w$ ,

$$\begin{cases} \kappa\phi_i^{n+\frac{1}{2}} = -L_i^{n+\frac{1}{2}}, \\ L_i^{n+\frac{1}{2}} = \kappa_B\partial_n f_i^{n+\frac{1}{2}} + \mathcal{M}_s\epsilon\frac{S(\phi_i^{n+\frac{1}{2}})-S_0}{S_0}\partial_n\phi_i^{n+\frac{1}{2}}, \\ -l_s^{-1}u_{\tau_j}^{n+\frac{1}{2}} = \boldsymbol{\tau}_j \cdot (\eta^n(\nabla\mathbf{u}^{n+\frac{1}{2}} + (\nabla\mathbf{u}^{n+\frac{1}{2}})^T) + \sum_i \lambda_i^{n+\frac{1}{2}}\delta_{\epsilon_i}\mathcal{P}_i^n) \cdot \mathbf{n} \\ \quad - \sum_i L_i^{n+\frac{1}{2}}\partial_{\tau_j}\phi_i^{n+\frac{1}{2}}, \quad j = 1, 2, \\ f_i^{n+\frac{1}{2}} = 0, \\ \partial_n\lambda_i^{n+\frac{1}{2}} = 0, \end{cases} \quad (43)$$

with  $(\cdot)^{n+\frac{1}{2}} = \frac{(\cdot)^n + (\cdot)^{n+1}}{2}$  and  $\mathcal{P}_i^n = I - \mathbf{n}_m^n \otimes \mathbf{n}_m^n$  with  $\mathbf{n}_m^n = \frac{\nabla\phi_i^n}{|\nabla\phi_i^n|}$  and

$$\begin{cases} f(\phi_i^{n+1}, \phi_i^n) = -\epsilon\Delta\phi_i^{n+\frac{1}{2}} + \frac{1}{4\epsilon}((\phi_i^{n+1})^2 + (\phi_i^n)^2 - 2)(\phi_i^{n+1} + \phi_i^n), \\ g(\phi_i^{n+1}, \phi_i^n) = \left(-\Delta f_i^{n+\frac{1}{2}} + \frac{1}{\epsilon^2}((\phi_i^{n+1})^2 + (\phi_i^n)^2 + \phi_i^{n+1}\phi_i^n - 1)f_i^{n+\frac{1}{2}}\right), \\ H_i^n = q_1(\phi_i^n + 1)^2 \sum_{j \neq i} [(\phi_j^{n+\frac{1}{2}} + 1)^2] - q_2((\phi_i^n)^2 - 1)^2 \sum_{j \neq i} [((\phi_j^{n+\frac{1}{2}})^2 - 1)^2], \\ H_i^{n+1} = q_1(\phi_i^{n+1} + 1)^2 \sum_{j \neq i} [(\phi_j^{n+\frac{1}{2}} + 1)^2] - q_2((\phi_i^{n+1})^2 - 1)^2 \sum_{j \neq i} [((\phi_j^{n+\frac{1}{2}})^2 - 1)^2], \\ f_w(\phi^n) = q_{w_1}(\phi_i^n + 1)^2(\phi_w + 1)^2 - q_{w_2}((\phi_i^n)^2 - 1)((\phi_w)^2 - 1). \end{cases} \quad (44)$$

Thus we have

$$\begin{aligned} \frac{H_i^{n+1} - H_i^n}{\phi_i^{n+1} - \phi_i^n} &= \frac{1}{\phi_i^{n+1} - \phi_i^n} \left( q_1(\phi_i^{n+1} + 1)^2 \sum_{j \neq i} [(\phi_j^{n+\frac{1}{2}} + 1)^2] - q_2((\phi_i^{n+1})^2 - 1)^2 \sum_{j \neq i} [((\phi_j^{n+\frac{1}{2}})^2 - 1)^2] \right. \\ &\quad \left. - q_1(\phi_i^n + 1)^2 \sum_{j \neq i} [(\phi_j^{n+\frac{1}{2}} + 1)^2] + q_2((\phi_i^n)^2 - 1)^2 \sum_{j \neq i} [((\phi_j^{n+\frac{1}{2}})^2 - 1)^2] \right) \\ &= q_1(\phi_i^{n+1} + \phi_i^n + 2) \sum_{j \neq i} [(\phi_j^{n+\frac{1}{2}} + 1)^2] \\ &\quad - q_2(\phi_i^{n+1} + \phi_i^n)((\phi_i^{n+1})^2 + (\phi_i^n)^2 - 2) \sum_{j \neq i} [((\phi_j^{n+\frac{1}{2}})^2 - 1)^2] \end{aligned} \quad (45)$$

Similarly,

$$\begin{aligned} \frac{f_w(\phi_i^{n+1}) - f_w(\phi_i^n)}{\phi_i^{n+1} - \phi_i^n} &= q_{w_1}(\phi_i^{n+1} + \phi_i^n + 2)(\phi_w + 1)^2 \\ &\quad - q_{w_2}(\phi_i^{n+1} + \phi_i^n)((\phi_i^{n+1})^2 + (\phi_i^n)^2 - 2)(\phi_w^2 - 1)^2 \end{aligned} \quad (46)$$

Later on, we keep the form  $\frac{f_w(\phi_i^{n+1}) - f_w(\phi_i^n)}{\phi_i^{n+1} - \phi_i^n}$  and  $\frac{H(\phi_i^{n+1}) - H(\phi_i^n)}{\phi_i^{n+1} - \phi_i^n}$  for convenience in later derivation.

The above scheme obeys the following theorem of energy stability.

**Theorem 3.1.** *If  $(\phi_i^n, \mu_i^n, \mathbf{u}^n, P^n)$  are smooth solutions of the above system (42)-(43), then the following energy law is satisfied:*

$$\begin{aligned} \mathcal{E}_{total}^{n+1} - \mathcal{E}_{total}^n &= (\mathcal{E}_{kin}^{n+1} + \sum_i^N [\mathcal{E}_{cell_i}^{n+1} + \mathcal{E}_{i,int}^{n+1} + \mathcal{E}_{w_i}^{n+1}]) - (\mathcal{E}_{kin}^n + \sum_i^N [\mathcal{E}_{cell_i}^n + \mathcal{E}_{i,int}^n + \mathcal{E}_{w_i}^n]) \\ &= \frac{\Delta t}{Re} \left( -2\|(\eta^n)^{1/2}\mathbf{D}_\eta^{n+\frac{1}{2}}\|^2 - \mathcal{M} \sum_i^N \|\nabla\mu_i^{n+\frac{1}{2}}\|^2 - \xi \sum_i^N \|\epsilon\phi_i^n \nabla\lambda_i^{n+\frac{1}{2}}\|^2 \right) \end{aligned}$$

$$-\frac{1}{\kappa} \left\| \sum_i^N L(\phi_i^{n+\frac{1}{2}}) \right\|_w^2 - \|l_s^{-1/2} \mathbf{u}_\tau^{n+\frac{1}{2}}\|_w^2 \right), \quad (47)$$

where  $\mathcal{E}_{total}^n = \mathcal{E}_{kin}^n + \sum_i^N [\mathcal{E}_{cell_i}^n + \mathcal{E}_{i,int}^n + \mathcal{E}_{w_i}^n]$  with  $\mathcal{E}_{kin}^n = \frac{1}{2} \|\mathbf{u}^n\|^2$ ,  $\mathcal{E}_{cell_i}^n = \frac{\kappa_B \|f_i^n\|^2}{2Re\epsilon} + \mathcal{M}_s \frac{(S(\phi_i^n) - S(\phi_{i,0}))^2}{2ReS(\phi_{i,0})} + \frac{\alpha}{Re} H_i^n$  and  $\mathcal{E}_{i,w}^n = \frac{\alpha}{Re} \int_\Omega f_{i,w}^n d\mathbf{x}$ .

The following two lemmas are needed for proving **Theorem 3.1**. Proof of these two lemmas can be found in [39].

**Lemma 3.2.** *Let*

$$f(\phi^{n+1}, \phi^n) = -\epsilon \Delta \phi^{n+\frac{1}{2}} + \frac{1}{4\epsilon} ((\phi^{n+1})^2 + (\phi^n)^2 - 2)(\phi^{n+1} + \phi^n). \quad (48)$$

Then  $f(\phi^{n+1}, \phi^n)$  satisfies

$$\int_\Omega f(\phi^{n+1}, \phi^n) (\phi^{n+1} - \phi^n) d\mathbf{x} = S^{n+1} - S^n - \int_{\partial\Omega_w} \epsilon \partial_n \phi^{n+\frac{1}{2}} (\phi^{n+1} - \phi^n) ds, \quad (49)$$

where  $S^{n+1} = \int_\Omega G(\phi^{n+1}) d\mathbf{x}$ ,  $S^n = \int_\Omega G(\phi^n) d\mathbf{x}$ .

**Lemma 3.3.** *Let  $g(\phi^{n+1}, \phi^n) = -\Delta f^{n+\frac{1}{2}} + \frac{1}{\epsilon^2} ((\phi^{n+1})^2 + (\phi^n)^2 + \phi^{n+1} \phi^n - 1) f^{n+\frac{1}{2}}$ . Then  $g(\phi^{n+1}, \phi^n)$  satisfies*

$$\begin{aligned} & \int_\Omega g(\phi^{n+1}, \phi^n) (\phi^{n+1} - \phi^n) d\mathbf{x} \\ &= \int_\Omega \frac{1}{2\epsilon} ((f^{n+1})^2 - (f^n)^2) d\mathbf{x} - \int_{\partial\Omega_w} \partial_n f^{n+\frac{1}{2}} (\phi^{n+1} - \phi^n) ds, \end{aligned} \quad (50)$$

where  $f^{n+1} = -\epsilon \Delta \phi^{n+1} + \frac{1}{\epsilon} ((\phi^{n+1})^2 - 1) \phi^{n+1}$ ,  $f^n = -\epsilon \Delta \phi^n + \frac{1}{\epsilon} ((\phi^n)^2 - 1) \phi^n$ .

**Proof of Theorem 3.1:** Multiplying the first equation in system (42) by  $\Delta t \mathbf{u}^{n+\frac{1}{2}}$  gives

$$\begin{aligned} & \int_\Omega \frac{1}{2} ((\mathbf{u}^{n+1})^2 - (\mathbf{u}^n)^2) d\mathbf{x} + \int_\Omega \Delta t \mathbf{u}^{n+\frac{1}{2}} \cdot ((\mathbf{u}^{n+\frac{1}{2}} \nabla) \cdot \mathbf{u}^{n+\frac{1}{2}}) d\mathbf{x} \\ & - \frac{\Delta t}{Re} \int_\Omega P^{n+\frac{1}{2}} \nabla \cdot \mathbf{u}^{n+\frac{1}{2}} d\mathbf{x} \\ &= -\frac{\Delta t}{Re} \int_\Omega \nabla \mathbf{u}^{n+\frac{1}{2}} : \eta^n (\nabla \mathbf{u}^{n+\frac{1}{2}} + (\nabla \mathbf{u}^{n+\frac{1}{2}})^T) d\mathbf{x} + \frac{\Delta t}{Re} \sum_i \int_\Omega \mathbf{u}^{n+\frac{1}{2}} \cdot \nabla \phi_i^{n+1} \mu_i^{n+1} d\mathbf{x} \\ & - \frac{\Delta t}{Re} \sum_i \int_\Omega \lambda_i \delta_{\epsilon_i} \mathcal{P}_i^n : \nabla \mathbf{u}^{n+\frac{1}{2}} d\mathbf{x} + \frac{\Delta t}{Re} \sum_i \int_{\partial\Omega_w} \lambda_i^{n+\frac{1}{2}} (\delta_{\epsilon_i} \mathcal{P}_i^n \cdot \mathbf{n}) \cdot \mathbf{u}_\tau^{n+\frac{1}{2}} ds \\ & + \frac{\Delta t}{Re} \int_{\partial\Omega_w} \mathbf{u}^{n+\frac{1}{2}} \cdot \eta^n ((\nabla \mathbf{u}^{n+\frac{1}{2}} + (\nabla \mathbf{u}^{n+\frac{1}{2}})^T) \cdot \mathbf{n}) ds. \end{aligned} \quad (51)$$

Multiplying the fourth equation in system (42) by  $\frac{\phi_i^{n+1} - \phi_i^n}{Re}$  and integration by parts lead to

$$\begin{aligned} & \frac{1}{Re} \sum_i \int_\Omega \mu_i^{n+1/2} (\phi_i^{n+1} - \phi_i^n) d\mathbf{x} = \frac{\kappa_B}{Re} \sum_i \int_\Omega \frac{1}{2\epsilon} ((f_i^{n+1})^2 - (f_i^n)^2) d\mathbf{x} \\ & + \frac{\mathcal{M}_s (S(\phi_i^{n+1}) - S_{i,0})^2 - (S(\phi_i^n) - S_{i,0})^2}{2S_{i,0}} + \frac{\alpha}{Re} \sum_i \int_\Omega (H_i^{n+1} - H_i^n) d\mathbf{x} + \frac{\alpha}{Re} \sum_i \int_\Omega (f_w(\phi_i^{n+1}) - f_w(\phi_i^n)) d\mathbf{x} \end{aligned} \quad (52)$$

$$-\frac{\kappa_B}{Re} \sum_i \int_{\partial\Omega_w} \partial_n f_i^{n+\frac{1}{2}} (\phi_i^{n+1} - \phi_i^n) ds - \frac{\mathcal{M}_s}{Re} \sum_i \int_{\partial\Omega_w} \frac{S(\phi_i^{n+\frac{1}{2}}) - S_{i,0}}{S_{i,0}} \epsilon \partial_n \phi_i^{n+\frac{1}{2}} (\phi_i^{n+1} - \phi_i^n) ds .$$

Multiplying the third equation in system (42) by  $\frac{\mu_i^{n+\frac{1}{2}} \Delta t}{Re}$  yield

$$\begin{aligned} & \frac{1}{Re} \sum_i \int_{\Omega} \mu_i^{n+\frac{1}{2}} (\phi_i^{n+1} - \phi_i^n) d\mathbf{x} + \frac{\Delta t}{Re} \sum_i \int_{\Omega} \mu_i^{n+\frac{1}{2}} (\mathbf{u}^{n+\frac{1}{2}} \cdot \nabla) \phi_i^{n+\frac{1}{2}} d\mathbf{x} \\ &= -\frac{\mathcal{M} \Delta t}{Re} \sum_i \int_{\Omega} (\nabla \mu_i^{n+\frac{1}{2}})^2 d\mathbf{x} . \end{aligned} \quad (53)$$

Multiplying the last equation in system (42) by  $\frac{\lambda_i^{n+\frac{1}{2}} \Delta t}{Re}$  and integration by parts then sum by  $i$  give

$$\frac{\Delta t}{Re} \sum_i \int_{\Omega} (\lambda_i^{n+\frac{1}{2}} \delta_{\epsilon_i} \mathcal{P}_i^n) : \nabla \mathbf{u}^{n+\frac{1}{2}} d\mathbf{x} - \frac{\Delta t}{Re} \sum_i \int_{\Omega} \xi \epsilon^2 (\phi_i^n)^2 \left| \nabla \lambda_i^{n+\frac{1}{2}} \right|^2 d\mathbf{x} = 0 . \quad (54)$$

The discretized energy dissipation law (47) is obtained by combining Eqs. (51)-(54) and organizing the terms according to the boundary conditions  $L(\phi_i)$  as shown in (43).  $\blacksquare$

### 3.2. Fully discrete $C^0$ finite element scheme

The spatial discretization using  $C^0$  finite element is straight forward. Let  $\Omega$  be the domain of interest with a Lipschitz-continuous boundary  $\partial\Omega$ . Let  $\mathbf{W}_b^h \subset \mathbf{W}_b$  be a finite element space with respect to the triangulation of the domain  $\Omega$ . The fully discrete scheme of the system is to find

$$(\{\Phi_h\}^{n+1}, \{\mathbf{U}\}_h^{n+1}, \{F_h\}^{n+1}, \{\Lambda_h\}^{n+1}, \{p_h\}^{n+1}, \{\mathbf{u}_h\}^{n+1}) \in \mathbf{W}_b^h,$$

such that for any  $(\psi_{1,h}, \dots, \psi_{N,h}, \chi_{1,h}, \dots, \chi_{N,h}, \zeta_{1,h}, \dots, \zeta_{N,h}, \Theta_{1,h}, \dots, \Theta_{N,h}, q_h, \mathbf{v}_h) \in \mathbf{W}_b^h$ , the following scheme holds.

$$\left\{ \begin{aligned} & \int_{\Omega} \left( \frac{\mathbf{u}_h^{n+1} - \mathbf{u}_h^n}{\Delta t} + (\mathbf{u}_h^{n+\frac{1}{2}} \cdot \nabla) \mathbf{u}_h^{n+\frac{1}{2}} + \frac{1}{Re} \nabla P_h^{n+\frac{1}{2}} \right) \cdot \mathbf{v}_h d\mathbf{x} \\ &= - \int_{\Omega} \frac{1}{Re} (\eta_h^n (\nabla \mathbf{u}_h^{n+\frac{1}{2}} + (\nabla \mathbf{u}_h^{n+\frac{1}{2}})^T)) : \nabla \mathbf{v}_h d\mathbf{x} \\ & \quad + \sum_i \int_{\Omega} \frac{1}{Re} \mu_{i,h}^{n+\frac{1}{2}} \nabla \phi_h^{n+\frac{1}{2}} \cdot \mathbf{v}_h d\mathbf{x} - \sum_i \int_{\Omega} \frac{1}{Re} \lambda_{i,h}^{n+\frac{1}{2}} \mathcal{P}_{i,h}^n \delta_{i,h,\epsilon} : \mathbf{v}_h d\mathbf{x} \\ & \quad + \int_{\partial\Omega_w} \frac{1}{Re} \mathbf{n} \cdot (\eta_h^n (\nabla \mathbf{u}_h^{n+\frac{1}{2}} + (\nabla \mathbf{u}_h^{n+\frac{1}{2}})^T) + \sum_i \lambda_{i,h}^{n+\frac{1}{2}} \mathcal{P}_{i,h}^n \delta_{i,\epsilon}) \cdot \mathbf{v}_h d\mathbf{x} , \\ & \int_{\Omega} (\nabla \cdot \mathbf{u}_h^{n+\frac{1}{2}}) q_h d\mathbf{x} = 0 , \\ & \int_{\Omega} \left( \frac{\phi_{i,h}^{n+1} - \phi_{i,h}^n}{\Delta t} + (\mathbf{u}_h^{n+\frac{1}{2}} \cdot \nabla) \phi_{i,h}^{n+\frac{1}{2}} \right) \psi_{i,h} d\mathbf{x} = - \int_{\Omega} \mathcal{M} \nabla \mu_{i,h}^{n+\frac{1}{2}} \nabla \psi_{i,h} d\mathbf{x} , \\ & \int_{\Omega} \mu_{i,h}^{n+\frac{1}{2}} \chi_{i,h} d\mathbf{x} = \int_{\Omega} \left( \kappa_B \frac{1}{\epsilon^2} ((\phi_{i,h}^{n+1})^2 + (\phi_{i,h}^n)^2 + \phi_{i,h}^{n+1} \phi_{i,h}^n - 1) f_{i,h}^{n+\frac{1}{2}} \right. \\ & \quad \left. + \mathcal{M}_s \frac{(S(\phi_{i,h}^{n+\frac{1}{2}}) - S(\phi_{i,h,0}))}{S(\phi_{i,h,0})} \left( \frac{1}{4\epsilon} ((\phi_{i,h}^{n+1})^2 + (\phi_{i,h}^n)^2 - 2)(\phi_{i,h}^{n+1} + \phi_{i,h}^n) \right) \right) \chi_{i,h} d\mathbf{x} \\ & \quad + \int_{\Omega} (\kappa_B \nabla f_{i,h}^{n+\frac{1}{2}} + \mathcal{M}_s \epsilon \frac{(S(\phi_{i,h}^{n+\frac{1}{2}}) - S(\phi_{i,h,0}))}{S(\phi_{i,h,0})} \nabla \phi_{i,h}^{n+\frac{1}{2}}) \cdot \nabla \chi_{i,h} d\mathbf{x} \\ & \quad + \int_{\Omega} \alpha \frac{f_w(\phi_{i,h}^{n+1}) - f_w(\phi_{i,h}^n)}{\phi_{i,h}^{n+1} - \phi_{i,h}^n} \chi_{i,h} d\mathbf{x} + \int_{\Omega} \alpha \frac{(H_{i,h}^{n+1} - H_{i,h}^n)}{\phi_{i,h}^{n+1} - \phi_{i,h}^n} \chi_{i,h} d\mathbf{x} \\ & \quad - \int_{\partial\Omega_w} (\kappa_B \partial_n f_{i,h}^{n+\frac{1}{2}} + \mathcal{M}_s \epsilon \frac{(S(\phi_{i,h}^{n+\frac{1}{2}}) - S(\phi_{i,h,0}))}{S(\phi_{i,h})} \partial_n \phi_{i,h}^{n+\frac{1}{2}}) \chi_{i,h} ds , \\ & \int_{\Omega} f_{i,h}^{n+\frac{1}{2}} \zeta_{i,h} = \int_{\Omega} \epsilon \nabla \phi_{i,h}^{n+\frac{1}{2}} \cdot \nabla \zeta_{i,h} + \int_{\Omega} \frac{1}{\epsilon} ((\phi_{i,h}^{n+\frac{1}{2}})^2 - 1) \phi_{i,h}^{n+\frac{1}{2}} \zeta_{i,h} d\mathbf{x} \\ & \quad - \int_{\partial\Omega_w} \epsilon \partial_n \phi_{i,h}^{n+\frac{1}{2}} \zeta_{i,h} d\mathbf{x} , \\ & \int_{\Omega} \delta_{i,h,\epsilon} \mathcal{P}_{i,h}^n : \nabla \mathbf{u}_{i,h}^{n+\frac{1}{2}} \Theta_{i,h} d\mathbf{x} - \int_{\Omega} \xi \epsilon^2 ((\phi_{i,h}^n)^2 \nabla \lambda_{i,h}^{n+\frac{1}{2}}) \cdot \nabla \Theta_{i,h} d\mathbf{x} + \int_{\partial\Omega_w} \xi \epsilon^2 ((\phi_{i,h}^n)^2 \partial_n \lambda_{i,h}^{n+\frac{1}{2}}) \Theta_{i,h} d\mathbf{x} = 0 . \end{aligned} \right. \quad (55)$$

Newton's iteration method is applied to solve the above nonlinear system. The unique solubility of (55) can be proved by following the idea introduced in [39].

#### 4. Numerical Results

In this section, we first calibrate the model parameters and validate the model by comparing with the experimental data on RBC deformation under different stretching forces. Then cell-wall interaction simulations are used to study the effects of adhesion force and local inextensibility. The energy stability of the numerical scheme is also illustrated. Then the calibrated model is used to study the cell-wall interaction and cell-cell aggregation.

##### 4.1. BenchMark: vesicle deformation under stretch

Laboratory experiments have tested the non-linear elasticity and deformation of RBC [55] in which optical tweezers are used to provide stretching force to the cells. We set up a numerical simulation mimicking RBC deformation in the experiment. New phases  $\phi_{tw_1}, \phi_{tw_2}$  are introduced to represent optical tweezers. The energy corresponding to optical tweezers stretching RBC is defined as:

$$H_{tw_i} = Q_{tw_1}(\phi_1 + 1)^2(\phi_{tw_i} + 1)^2 - Q_{tw_2}(\phi_1^2 - 1)^2(\phi_{tw_i}^2 - 1)^2, \quad i = 1, 2, \quad (56)$$

where  $Q_{tw}$  is a coefficient that controls the attraction (???) force that the optical tweezers provide. The value of other parameters are listed as follows:  $Re = 2 \times 10^{-4}, \mathcal{M} = 0.25, \kappa_B = 2 \times 10^{-3}, k = 2 \times 10^{-12}, l_s = 5 \times 10^{-3}, \mathcal{M}_s = 2$ . The force applied on the cell is calculated by the following equation:

$$\mathbf{F} = \int_{\Omega} \frac{\partial H_{tw_i}}{\partial \phi} \nabla \phi d\mathbf{x}. \quad (57)$$

The curves of axial and transverse diameter versus stretching forces are shown in Figure 3 together with the experimental data (diamonds with bars) from [55]. The results show that our model fits the experimental data very well.

##### 4.2. Cell-wall attraction

Cell-wall interactions under blood flow conditions play important roles during blood clotting [56] and cancer cell invasion [10]. This example is used to investigate the effect of adhesion force on the vesicle-wall interaction. We first consider the case without external flow. As shown in Figure 4, a vesicle is initially placed at a location with a point-wise contact with the wall phase. The parameter values of this simulation are listed as follows:  $Re = 2 \times 10^{-4}, \mathcal{M} = 5 \times 10^{-4}, \kappa_B = 2 \times 10^{-2}, \varepsilon = 2 \times 10^{-3}, \mathcal{M}_s = 10^2, k = 4 \times 10^{-11}, l_s = 5 \times 10^{-6}, \alpha = 1000, q_{w_1} = 2, q_{w_2} = 1$ .

Figure 5 shows the scenarios of the the vesicle with and without local inextensibility at different time. As shown in Fig. 6, the local inextensibility constrains slows down the deformation of the vesicle. For vesicle without local constrain, it allowed the membrane attached to the wall to be stretched (red color in Fig.6) to achieve the equilibrium faster. This also could be seen in the Fig. 7. It confirms that in both cases, the energy monotonously decays to the same value while the vesicle without local inextensibility evolves faster.

Then the effect of the strength of the adhesion force on the equilibrium profiles of the vesicles are illustrated in Figure 8. As expected, when the strength increases from 400 to 2500, the contact surface area increases.

During the blood clotting, the platelets interact with several coagulation factors and get activated. The full activated plated has strong adhesion force with vessel wall in order to stop bleeding more efficiently. In Figure 9, we simulate two platelets under the shear blood flow, one fully activated with strong adhesion and one partial activated with weak adhesion with vessel wall. It shows that when the fully activated one is captured by the wall; while the partial activated one is washed away by the shear flow.

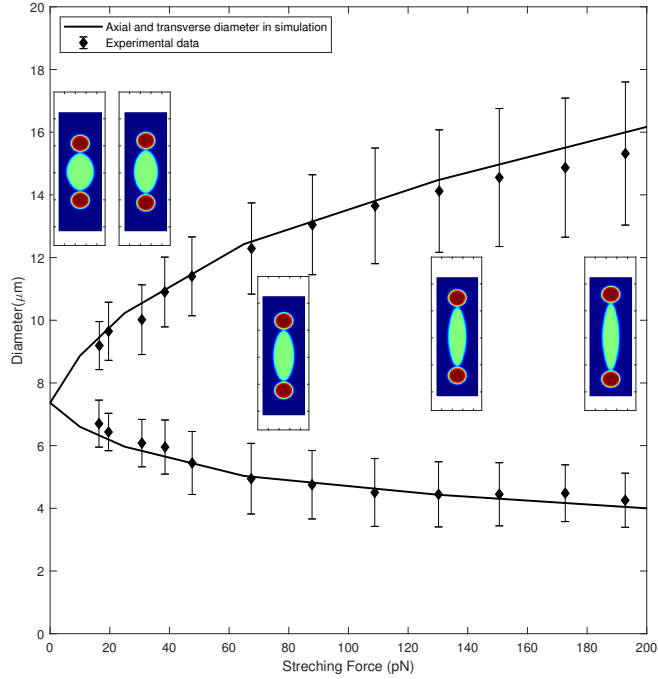


Figure 3: Nonlinear elastic deformation of red blood cell. The curve shows the change of the diameter versus stretching force. The diamond is the experiment data published in [55]. In the experiment schematic diagram, the centered phase is set to be the cell and the circulate area on the two side stands for the light tweezers. The force applied on the membrane is kept a constant when the tweezers moving. The equilibrium is reached when the membrane no longer extends under the certain stretch force.

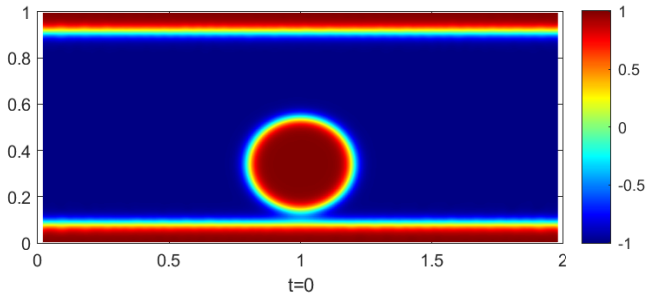


Figure 4: The initial state of the case.

#### 4.3. Cell aggregation and offset

Aggregation of red blood cell is a phenomenon observed in experiment [1]. In this part, we set up a simulation with four red blood cells contacted with each other at a small point. The parameters are shown below.  $Re = 2 \times 10^{-5}$ ,  $\mathcal{M} = 5 \times 10^{-4}$ ,  $\kappa_B = 4 \times 10^{-2}$ ,  $k = 4 \times 10^{-12}$ ,  $l_s = 5 \times 10^{-3}$ ,  $\mathcal{M}_s = 10^3$ ,  $\alpha = 3 \times 10^3$ ,  $q_1 = 1$ ,  $q_2 = 0.5$ . The evolution of the system with time is shown in 10.

From the result we can see that they are creeping together with time under the attractive force and form rouleaux which is consistent with the experimental result shown in [1] and [13].

Also, the deformation of the cells at equilibrium is related to the value of the attractive force [13, 11, 17]. Fig. 11 shows the status of moderately and strongly aggregate. The parameters are shown below.  $Re =$



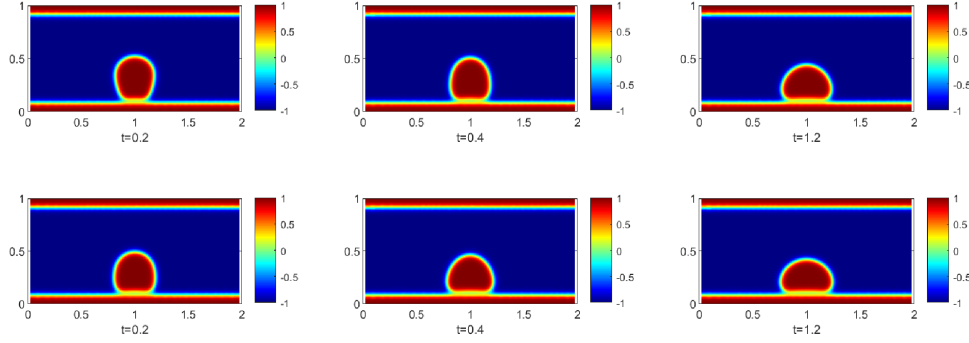


Figure 5: The top three pictures shows the deformation of the vesicle with local inextensibility. The bottom three pictures shows the deformation of the vesicle without local inextensibility.

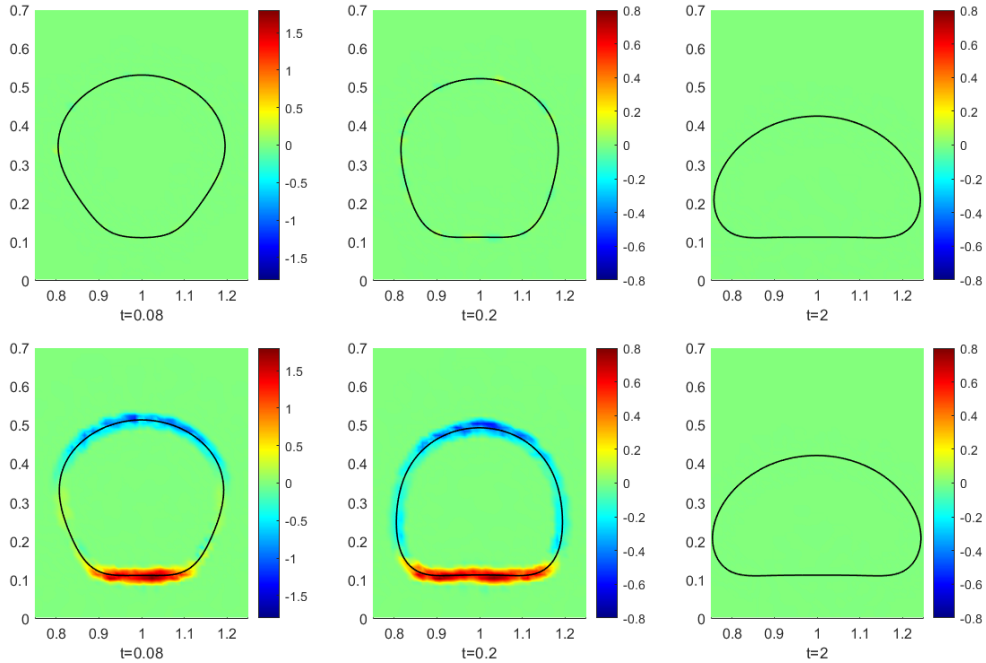


Figure 6: The top two pictures shows the value of surface divergence  $\mathcal{P}_i : \nabla \mathbf{u}$  with local inextensibility. The bottom pictures shows the surface divergence of the vesicle without local inextensibility.

$2 \times 10^{-4}$ ,  $\mathcal{M} = 5 \times 10^{-4}$ ,  $\kappa_B = 2 \times 10^{-2}$ ,  $k = 2 \times 10^{-11}$ ,  $l_s = 5 \times 10^{-3}$ ,  $\mathcal{M}_s = 10$ .

From the figure we can see that under strong aggregation force, obvious terminal hemispherical caps is shown and the offset between each adjacent cell is smaller as well. This result is consistent with the experimental phenomenon observed well [1]. In the following test we set the cells on a Couette flow with shear rate equal to be  $20s^{-1}$  with dimension as in [14]. The motion of the cells are shown in figure 12. Under shear flow, the rouleaux with strong adhesion still aggregate together; while the one with weak adhesion is broken up by the shear flow, which is consistent with the results reported in [14].

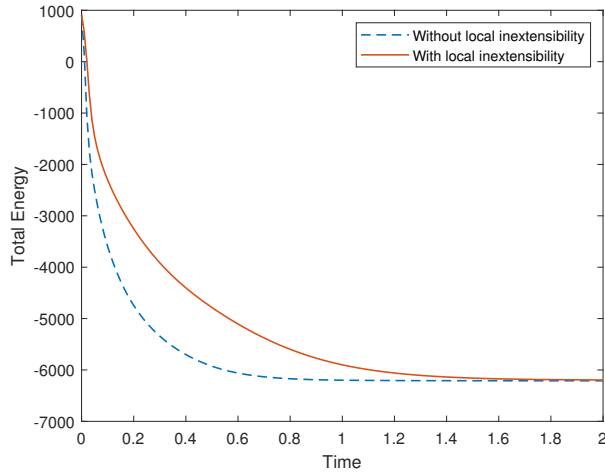


Figure 7: Total energy of the two system versus time.

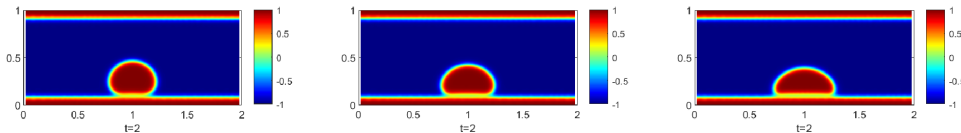


Figure 8: Equilibrium of the cells at different strength of the adhesion force. (Left:  $\alpha = 400$ ; Mid:  $\alpha = 1000$ ; Right:  $\alpha = 2500$ .)

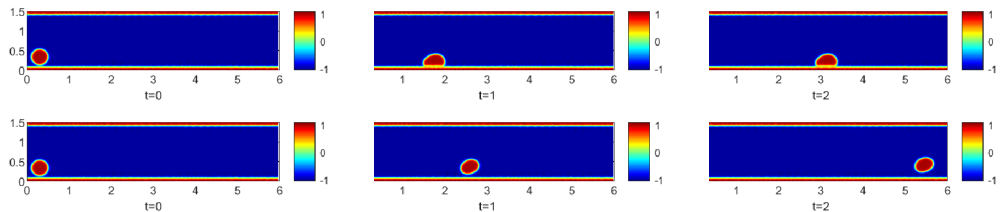


Figure 9: The top three picture shows the motion of the cell in strong adhesion case. The bottom three pictures shows the cell motion in weak adhesion case.

#### 4.4. Red blood cell motion at vessel bifurcation

In this part, we simulate the motion of RBCs in branched vessels. 4 cells are initially placed in the Y shaped vessel. Width of the main channel of the Y shaped vessel and the bottom branch of the vessel is set to be  $1 \times 10^{-7}$  meter. The top branch of the vessel is  $0.7 \times 10^{-7}$  meter, which is close to the size of a red blood cell. A pressure drop boundary condition is used to introduce a shear flow in the vessel with the velocity around  $5 \times 10^{-4} m/s$ , which is close to the blood flow in capillaries. Other model parameters in this simulation are as follows:  $Re = 2 \times 10^{-4}$ ,  $\mathcal{M} = 5 \times 10^{-4}$ ,  $\kappa_B = 4 \times 10^{-2}$ ,  $k = 4 \times 10^{-11}$ ,  $l_s = 2 = 5 \times 10^{-6}$ ,  $\mathcal{M}_s = 20$ .

Motion of the RBCs and the velocity field of the flow are shown in Figure 14, 15, and 13, respectively. We firstly simulate motion of the RBC group with a moderate aggregation force when they pass a Y-shaped channel with the same width of the both branches as a baseline. The cells divide equally at the vessel bifurcation. Then one of the channel is widen and a non-equal deviation is observed (3 move upwards, 1 moves downward) due to the lower resistance in the upper branch. Then, under the same geometric setup, a strong aggregation force is applied to the cells. In this case, all of the cells goes into the wider channel. The simulation result explains the experimental result in [1], which a great number of red blood cells are observed

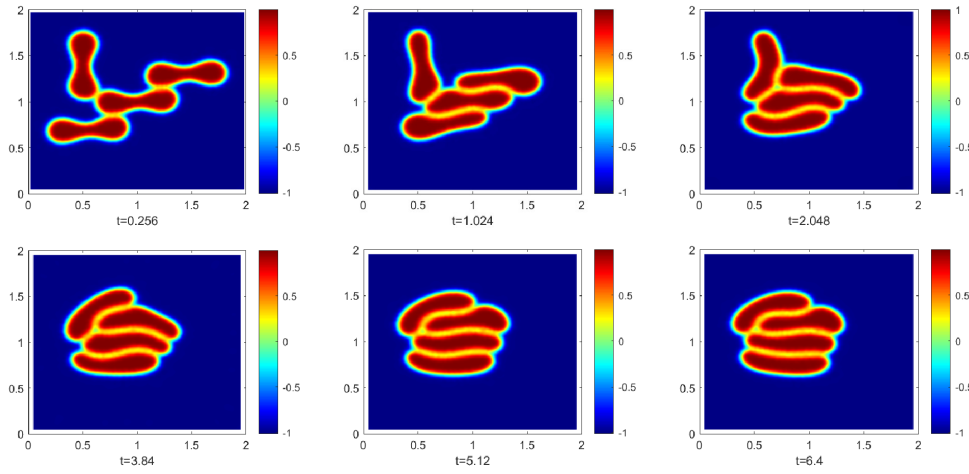


Figure 10: Aggregating of four red blood cells.

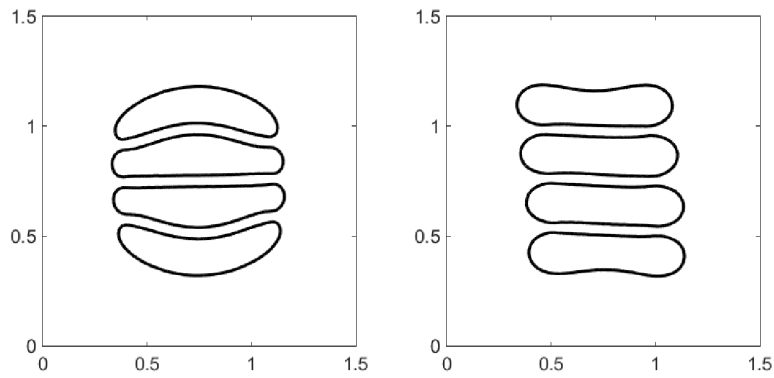


Figure 11: Left: Strong aggregate  $\alpha = 15 \times 10^3$ ,  $q_1 = 1$ ,  $q_2 = 1$ . Right: moderate aggregate  $\alpha = 100$ ,  $q_1 = 1$ ,  $q_2 = 1$ .

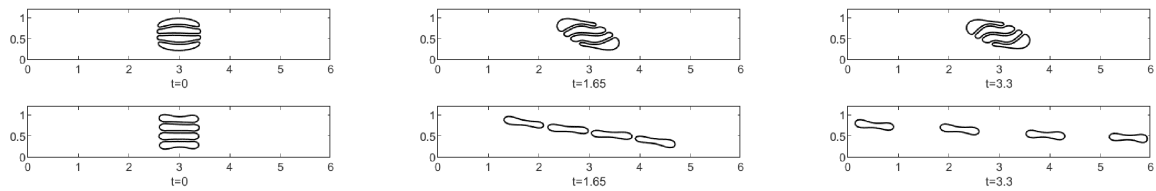


Figure 12: The top three figures shows the motion of the cells with strong aggregation. The bottom three figures shows the motion under moderate aggregation.

to be absent in the branched vessel under strong aggregate case compared with moderate aggregate.

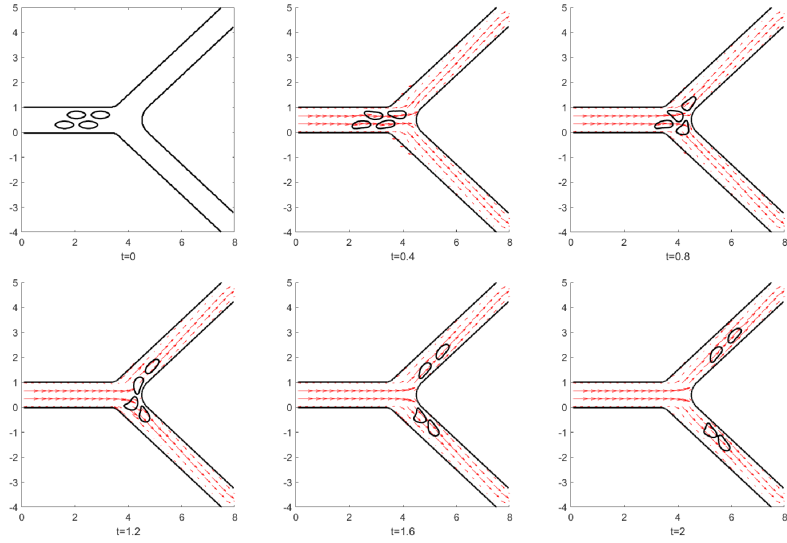


Figure 13: Cells are set in a cluster initially under a moderate aggregating force with  $\alpha = 25, q_1 = 1, q_2 = 1$ . The main channel width is 1 and the width of the two branches is 0.7. RBCs divide equally at the vessel bifurcation. The velocity field is indicated by the vector field.

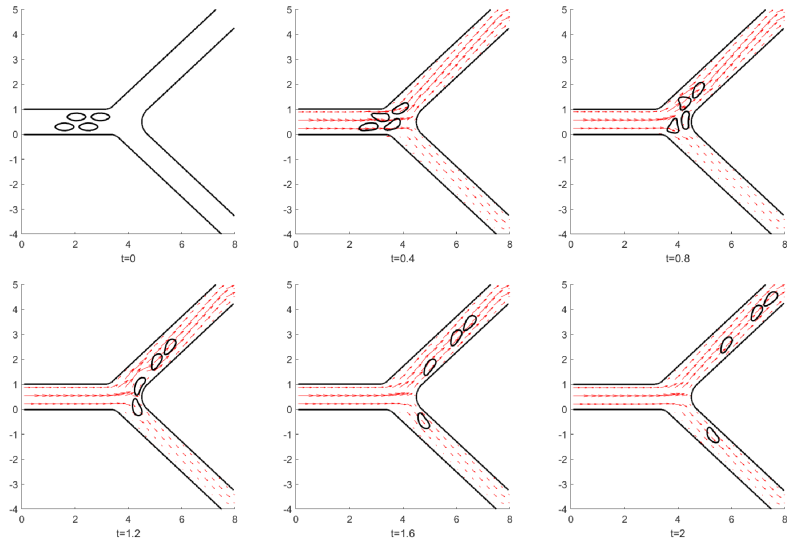


Figure 14: Cells are set in a cluster initially under a moderate aggregating force with  $\alpha = 25, q_1 = 1, q_2 = 1$ . The top branch is set to be 1 with the other stays 0.7. One of the cells is going into the branched vessel. The velocity field is shown as well.

## 5. Conclusions

In this paper, a thermodynamically consistent diffuse interface (phase-field) model for describing cell-wall, cell-cell interaction and aggregation is derived based on the energy variation method. The interactions of cellular and wall structures are modeled by introducing a new interaction energy with the help of the phase-field function.

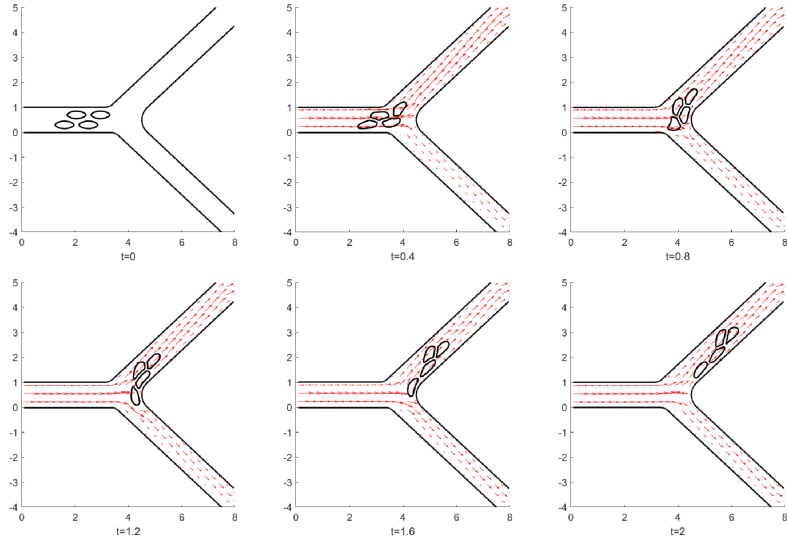


Figure 15: Cells are set in a cluster initially under a strong aggregating force with  $\alpha = 1.5 \times 10^3$ ,  $l_1 = 1$ ,  $Q_2 = 1$ . The set up is the same as Figure 14. None of the cells is going into the branched vessel. The velocity field is shown as well.

Then an efficient scheme using  $C^0$  finite element spatial discretization and the mid-point temporal discretization is proposed to solve the obtained model equations. Thanks to the mid-point temporal discretization, the obtained numerical scheme is unconditionally energy stable. The model and parameters are calibrated with experimental data on cell deformation under different stretch force. Then effects of the adhesion strength on cell-wall and cell-cell interaction are studied. In the end, the calibrated model is used to model red blood cell motion near the vessel bifurcation. The results are consistent with the experimental observation.

## References

- [1] T. Kirschkamp, H. Schmid-Schönbein, A. Weinberger, R. Smeets, Effects of fibrinogen and  $\alpha$ 2-macroglobulin and their apheretic elimination on general blood rheology and rheological characteristics of red blood cell aggregates, *Therapeutic Apheresis and Dialysis* 12 (5) (2008) 360–367.
- [2] A. L. Fogelson, K. B. Neeves, Fluid mechanics of blood clot formation, *Annual review of fluid mechanics* 47 (2015) 377–403.
- [3] K. Lee, M. Kinnunen, M. D. Khokhlova, E. V. Lyubin, A. V. Priezhev, I. Meglinski, A. A. Fedyanin, Optical tweezers study of red blood cell aggregation and disaggregation in plasma and protein solutions, *Journal of biomedical optics* 21 (3) (2016) 035001.
- [4] Y. Alapan, J. A. Little, U. A. Gurkan, Heterogeneous red blood cell adhesion and deformability in sickle cell disease, *Scientific reports* 4 (1) (2014) 1–8.
- [5] Y. Connor, Y. Tekleab, S. Tekleab, S. Nandakumar, D. Bharat, S. Sengupta, A mathematical model of tumor-endothelial interactions in a 3d co-culture, *Scientific reports* 9 (1) (2019) 1–14.
- [6] Y. Deng, D. P. Papageorgiou, X. Li, N. Perakakis, C. S. Mantzoros, M. Dao, G. E. Karniadakis, Quantifying fibrinogen-dependent aggregation of red blood cells in type 2 diabetes mellitus, *Biophysical journal* 119 (5) (2020) 900–912.
- [7] [Flow patterns around heart valves: A numerical method](#), *Journal of Computational Physics* 10 (2) (1972) 252–271. doi: [https://doi.org/10.1016/0021-9991\(72\)90065-4](https://doi.org/10.1016/0021-9991(72)90065-4). URL <https://www.sciencedirect.com/science/article/pii/0021999172900654>
- [8] C. S. Peskin, The immersed boundary method, *Acta Numerica* 11 (2002) 479–517. doi:10.1017/S0962492902000077.
- [9] A. L. Fogelson, R. D. Guy, Immersed-boundary-type models of intravascular platelet aggregation, *Computer methods in applied mechanics and engineering* 197 (25-28) (2008) 2087–2104.
- [10] A. Gerisch, M. A. Chaplain, Mathematical modelling of cancer cell invasion of tissue: local and non-local models and the effect of adhesion, *Journal of Theoretical Biology* 250 (4) (2008) 684–704.
- [11] P. Ziherl, S. Svetina, Flat and sigmoidally curved contact zones in vesicle-vesicle adhesion, *Proceedings of the National Academy of Sciences* 104 (3) (2007) 761–765.
- [12] Y. Liu, W. K. Liu, Rheology of red blood cell aggregation by computer simulation, *Journal of Computational Physics* 220 (1) (2006) 139–154.
- [13] P. Ziherl, Aggregates of two-dimensional vesicles: Rouleaux, sheets, and convergent extension, *Physical review letters* 99 (12) (2007) 128102.
- [14] J. Zhang, P. C. Johnson, A. S. Popel, Red blood cell aggregation and dissociation in shear flows simulated by lattice boltzmann method, *Journal of biomechanics* 41 (1) (2008) 47–55.
- [15] D. A. Fedosov, H. Noguchi, G. Gompper, Multiscale modeling of blood flow: from single cells to blood rheology, *Biomechanics and modeling in mechanobiology* 13 (2) (2014) 239–258.
- [16] Z. Xu, N. Chen, S. C. Shadden, J. E. Marsden, M. M. Kamocka, E. D. Rosen, M. Alber, Study of blood flow impact on growth of thrombi using a multiscale model, *Soft Matter* 5 (4) (2009) 769–779.
- [17] D. Flormann, O. Aouane, L. Kaestner, C. Ruloff, C. Misbah, T. Podgorski, C. Wagner, The buckling instability of aggregating red blood cells, *Scientific reports* 7 (1) (2017) 1–10.
- [18] B. Quaife, S. Veerapaneni, Y.-N. Young, Hydrodynamics and rheology of a vesicle doublet suspension, *Physical Review Fluids* 4 (10) (2019) 103601.
- [19] B. Quaife, S. Veerapaneni, Y.-N. Young, Hydrodynamics and rheology of a vesicle doublet suspension, *Physical Review Fluids* 4 (10) (2019) 103601.
- [20] D. M. Anderson, G. B. McFadden, A. A. Wheeler, [Diffuse-interface methods in fluid mechanics](#), *Annual Review of Fluid Mechanics* 30 (1) (1998) 139–165. arXiv:<https://doi.org/10.1146/annurev.fluid.30.1.139>, doi:10.1146/annurev.fluid.30.1.139. URL <https://doi.org/10.1146/annurev.fluid.30.1.139>
- [21] J. Lowengrub, L. Truskinovsky, Quasi-incompressible cah-hilliard fluids and topological transitions, *Proceedings of the Royal Society of London. Series A: Mathematical, Physical and Engineering Sciences* 454 (1978) (1998) 2617–2654. doi:10.1098/rspa.1998.0273.
- [22] Q. Du, C. Liu, R. Ryham, X. Wang, Energetic variational approaches in modeling vesicle and fluid interactions, *Physica D: Nonlinear Phenomena* 238 (9-10) (2009) 923–930.
- [23] Q. Du, C. Liu, R. Ryham, X. Wang, Modeling the spontaneous curvature effects in static cell membrane deformations by a phase field formulation, *Communications on Pure & Applied Analysis* 4 (3) (2005) 537.
- [24] X. Yang, V. Mironov, Q. Wang, Modeling fusion of cellular aggregates in biofabrication using phase field theories, *Journal of theoretical biology* 303 (2012) 110–118.
- [25] R. Gu, X. Wang, M. Gunzburger, Simulating vesicle-substrate adhesion using two phase field functions, *Journal of Computational Physics* 275 (2014) 626–641.
- [26] J. Zhang, S. Das, Q. Du, A phase field model for vesicle-substrate adhesion, *Journal of Computational Physics* 228 (20) (2009) 7837–7849.
- [27] S. Das, Q. Du, Adhesion of vesicles to curved substrates, *Physical Review E* 77 (1) (2008) 011907.
- [28] R. Gu, X. Wang, M. Gunzburger, A two phase field model for tracking vesicle-vesicle adhesion, *Journal of mathematical biology* 73 (5) (2016) 1293–1319.
- [29] J. Jiang, K. Garikipati, S. Rudraraju, A diffuse interface framework for modeling the evolution of multi-cell aggregates as a soft packing problem driven by the growth and division of cells, *Bulletin of mathematical biology* 81 (8) (2019) 3282–3300.

- [30] R. Gu, X. Wang, M. Gunzburger, A two phase field model for tracking vesicle–vesicle adhesion, *Journal of mathematical biology* 73 (5) (2016) 1293–1319.
- [31] Q. Du, C. Liu, R. Ryham, X. Wang, A phase field formulation of the willmore problem, *Nonlinearity* 18 (3) (2005) 1249.
- [32] F. Guillén-González, G. Tierra, Unconditionally energy stable numerical schemes for phase-field vesicle membrane model, *Journal of computational physics* 354 (2018) 67–85.
- [33] Q. Du, J. Zhang, Adaptive finite element method for a phase field bending elasticity model of vesicle membrane deformations, *SIAM Journal on Scientific Computing* 30 (3) (2008) 1634–1657.
- [34] Q. Cheng, J. Shen, Multiple scalar auxiliary variable (msav) approach and its application to the phase-field vesicle membrane model, *SIAM Journal on Scientific Computing* 40 (6) (2018) A3982–A4006.
- [35] J. Hua, P. Lin, C. Liu, Q. Wang, Energy law preserving c0 finite element schemes for phase field models in two-phase flow computations, *Journal of Computational Physics* 230 (19) (2011) 7115–7131.
- [36] P. Lin, C. Liu, Simulations of singularity dynamics in liquid crystal flows: A c0 finite element approach, *Journal of Computational Physics* 215 (1) (2006) 348–362.
- [37]
- [38] Z. Guo, P. Lin, A thermodynamically consistent phase-field model for two-phase flows with thermocapillary effects, *Journal of Fluid Mechanics* 766 (2015) 226–271.
- [39] L. Shen, Z. Xu, P. Lin, H. Huang, S. Xu, An energy stable c<sup>0</sup> finite element scheme for a phase-field model of vesicle motion and deformation, *SIAM Journal on Scientific Computing* 44 (1) (2022) B122–B145.
- [40] T. Qian, X.-P. Wang, P. Sheng, A variational approach to the moving contact line hydrodynamics, arXiv preprint cond-mat/0602293 (2006).
- [41] Q. Du, C. Liu, X. Wang, A phase field approach in the numerical study of the elastic bending energy for vesicle membranes, *Journal of Computational Physics* 198 (2) (2004) 450–468.
- [42] R. Chen, G. Ji, X. Yang, H. Zhang, Decoupled energy stable schemes for phase-field vesicle membrane model, *Journal of Computational Physics* 302 (2015) 509–523.
- [43] S. Aland, S. Egerer, J. Lowengrub, A. Voigt, Diffuse interface models of locally inextensible vesicles in a viscous fluid, *Journal of computational physics* 277 (2014) 32–47.
- [44] Z. Guo, F. Yu, P. Lin, S. Wise, J. Lowengrub, A diffuse domain method for two-phase flows with large density ratio in complex geometries, *Journal of Fluid Mechanics* 907 (2021).
- [45] K. C. Ong, M.-C. Lai, An immersed boundary projection method for simulating the inextensible vesicle dynamics, *Journal of Computational Physics* 408 (2020) 109277.
- [46] S. Xu, M. Alber, Z. Xu, Three-phase model of visco-elastic incompressible fluid flow and its computational implementation, *Communications in computational physics* 25 (2) (2019) 586.
- [47] B. Eisenberg, Y. Hyon, C. Liu, Energy variational analysis of ions in water and channels: Field theory for primitive models of complex ionic fluids, *The Journal of Chemical Physics* 133 (10) (2010) 104104.
- [48] Y. Hyon, C. Liu, et al., Energetic variational approach in complex fluids: maximum dissipation principle, *Discrete & Continuous Dynamical Systems* 26 (4) (2010) 1291.
- [49] S. Xu, P. Sheng, C. Liu, An energetic variational approach for ion transport, *Communications in Mathematical Sciences* 12 (4) (2014) 779–789.
- [50] M.-H. Giga, A. Kirshtein, C. Liu, Variational modeling and complex fluids, 2017.
- [51] S. Xu, B. Eisenberg, Z. Song, H. Huang, Osmosis through a semi-permeable membrane: a consistent approach to interactions, arXiv preprint arXiv:1806.00646 (2018).
- [52] T. Qian, X.-P. Wang, P. Sheng, A variational approach to moving contact line hydrodynamics, *Journal of Fluid Mechanics* 564 (2006) 333. doi:10.1017/S0022112006001935.
- [53] C. Liu, H. Wu, An energetic variational approach for the cahn–hilliard equation with dynamic boundary condition: model derivation and mathematical analysis, *Archive for Rational Mechanics and Analysis* (2019) 1–81.
- [54] Z. Guo, P. Lin, J. S. Lowengrub, A numerical method for the quasi-incompressible cahn–hilliard–navier–stokes equations for variable density flows with a discrete energy law, *Journal of Computational Physics* 276 (2014) 486–507.
- [55] J. Mills, L. Qie, M. Dao, C. Lim, S. Suresh, Nonlinear elastic and viscoelastic deformation of the human red blood cell with optical tweezers, *Molecular & Cellular Biomechanics* 1 (3) (2004) 169.
- [56] Z. Wu, Z. Xu, O. Kim, M. Alber, Three-dimensional multi-scale model of deformable platelets adhesion to vessel wall in blood flow, *Philosophical Transactions of the Royal Society A: Mathematical, Physical and Engineering Sciences* 372 (2021) 20130380.